AP-2α and AP-2β cooperatively function in the craniofacial surface ectoderm to regulate chromatin and gene expression dynamics during facial development.

Eric Van Otterloo[1,2,3,4,*], Isaac Milanda[4], Hamish Pike[4], Hong Li[4], Kenneth L Jones[5#], Trevor Williams[4,6,7,*]

[1] Iowa Institute for Oral Health Research, College of Dentistry & Dental Clinics, University of Iowa, Iowa City, IA, 52242, USA

[2] Department of Periodontics, College of Dentistry & Dental Clinics, University of Iowa, Iowa City, IA, 52242, USA

[3] Department of Anatomy and Cell Biology, Carver College of Medicine, University of Iowa, Iowa City, IA, 52242, USA

[4] Department of Craniofacial Biology, University of Colorado Anschutz Medical Campus, Aurora, CO, 80045, USA

[5] Department of Pediatrics, Section of Hematology, Oncology, and Bone Marrow Transplant, University of Colorado School of Medicine, University of Colorado Anschutz Medical Campus, Aurora, CO, 80045, USA

[6] Department of Cell and Developmental Biology, University of Colorado Anschutz Medical Campus, Aurora, CO, 80045, USA

[7] Department of Pediatrics, University of Colorado Anschutz Medical Campus, Children's Hospital Colorado, Aurora, CO 80045, USA

* Corresponding Authors

[#]Present Address: Department of Cell Biology, University of Oklahoma Health Sciences Center, Oklahoma City, OK 73104, USA

Keywords: Tfap2, AP-2, transcription factor, ectoderm, craniofacial, neural crest, Wnt signaling

ABSTRACT:

The facial surface ectoderm is essential for normal development of the underlying cranial neural crest cell populations, providing signals that direct appropriate growth, patterning, and morphogenesis. Despite the importance of the ectoderm as a signaling center, the molecular cues and genetic programs implemented within this tissue are understudied. Here we show that removal of two members of the AP-2 transcription factor family, AP-2α and AP-2ß, within the early embryonic ectoderm leads to major alterations in the mouse craniofacial complex. Significantly, there are clefts in both the upper face and mandible, accompanied by fusion of the upper and lower jaws in the hinge region. Comparison of ATAC-seq and RNA-seq analyses between controls and mutants revealed significant changes in chromatin accessibility and gene expression centered on multiple AP-2 binding motifs associated with enhancer elements within these ectodermal lineages. In particular, loss of these AP-2 proteins affects both skin differentiation as well as multiple signaling pathways, most notably the WNT pathway. The role of reduced Wnt signaling throughput in the mutant phenotype was further confirmed using reporter assays and rescue experiments involving Wnt1 ligand overexpression. Collectively, these findings highlight a conserved ancestral function for AP-2 transcription factors in ectodermal development and signaling, and provide a framework from which to understand the gene regulatory network operating within this tissue that directs vertebrate craniofacial development.

INTRODUCTION

The development of the vertebrate face during embryogenesis requires the integration of gene regulatory programs and signaling interactions across different tissue layers to regulate normal growth and morphogenesis (Chai & Maxson, 2006; M. J. Dixon, Marazita, Beaty, & Murray, 2011). The bulk of the face is derived from neural crest cells (NCCs), which migrate into the nascent mandibular, maxillary, and frontonasal facial prominences. Recent studies have indicated the cranial NCCs (CNCCs), residing within distinct facial prominences, are molecularly similar, genetically poised, and awaiting additional signaling information for their continued development (Minoux et al., 2017; Minoux & Rijli, 2010). These critical signals are provided by surrounding and adjacent tissues, especially the forebrain, endoderm, and ectoderm (Le Douarin, Creuzet, Couly, & Dupin, 2004). With respect to the ectoderm, studies in chick have indicated the presence of a frontonasal ectodermal zone, defined by the juxtaposition of Fgf8 and Shh expressing domains, that can direct facial outgrowth and patterning (Hu & Marcucio, 2009; Hu, Marcucio, & Helms, 2003). The ectoderm is also a critical source of Wnt signaling that is required for continued facial outgrowth and patterning, exemplified by the lack of almost all craniofacial structures arising when Wntless/Gpr177 is removed from the facial ectoderm (Goodnough et al., 2014; Reynolds et al., 2019). Further evidence for an essential role of the ectoderm in craniofacial development comes from genetic analysis of pathology associated with human syndromic orofacial clefting. Specifically, mutations in *IRF6* (Kondo et al., 2002) and *GRHL3* (Peyrard-Janvid et al., 2014) are associated with van der Woude Syndrome, while *TRP63* mutations result in ectodermal dysplasias with associated facial clefting (Celli et al., 1999). Notably, all three of these human genes encode transcription factors which exhibit much stronger expression in the facial ectoderm than in the underlying neural crest (Hooper, Jones, Smith, Williams, & Li, 2020; Leach, Feng, & Williams, 2017). Studies of mouse facial dysmorphology have also shown the importance of additional genes with biased expression in the ectoderm—including *Sfn*, *Jag2*, *Wnt9b* and *Esrp1*—that regulate differentiation, signaling, and splicing (Bebee et al., 2015; Jiang et al., 1998; Jin, Han, Taketo, & Yoon, 2012; Lee, Kong, & Weatherbee, 2013; Lee et al., 2020; Richardson et al., 2006). Indeed, the interplay between surface ectoderm and underlying NCCs provides a molecular platform for the craniofacial diversity apparent within the vertebrate clade, but also serves as a system which is frequently disrupted to cause human craniofacial birth defects. Therefore, identifying

the regulatory mechanisms and factors involved in coordinating NCC:ectoderm interactions is a prerequisite for uncovering the molecular nodes susceptible to perturbation.

The AP-2 transcription family represent an intriguing group of regulatory molecules with strong links to ectodermal development (Eckert, Buhl, Weber, Jager, & Schorle, 2005). Indeed, previous analyses have indicated that AP-2 genes may be an ancestral transcriptional regulator of ectoderm development in chordates predating the development of the neural crest in the cephalochordate Amphioxus and the ascidian *Ciona* (Imai, Hikawa, Kobayashi, & Satou, 2017; Meulemans & Bronner-Fraser, 2002, 2004). Subsequently, it has been postulated that this gene family has been co-opted into the regulatory network required for neural crest development in the vertebrates, where it may serve as one of the master regulators of this lineage (Meulemans & Bronner-Fraser, 2002, 2004; Van Otterloo et al., 2012). Therefore, in vertebrates, AP-2 family expression is often observed in both the non-neural ectoderm as well as the neural crest. Amphioxus possesses a single AP-2 gene, but in mammals such as mouse and human there are five family members, *Tfap2a-e* encoding the proteins AP-2α-ε, respectively (Eckert et al., 2005; Meulemans & Bronner-Fraser, 2002). All mammalian AP-2 proteins have very similar DNA sequence preferences and bind as dimers to a consensus motif GCCNNNGGC, except for AP-2δ which is the least conserved family member (Badis et al., 2009; Williams & Tjian, 1991; Zhao, Satoda, Licht, Hayashizaki, & Gelb, 2001). Amongst these five genes, *Tfap2a* and *Tfap2b* show the highest levels of expression in the developing mouse embryonic facial tissues with lower levels of *Tfap2c* and essentially undetectable transcripts from *Tfap2d* and *Tfap2e* (Hooper et al., 2020; Van Otterloo, Li, Jones, & Williams, 2018). Importantly, mutations in human *TFAP2A* and *TFAP2B*, are also linked to the human conditions Branchio-Oculo-Facial Syndrome (Milunsky et al., 2008) and Char Syndrome (Satoda et al., 2000) respectively, conditions which both have a craniofacial component. *TFAP2A* has also been linked to non-syndromic orofacial clefting (MIM 119530) (A. F. Davies et al., 1995; S. J. Davies et al., 2004).

Previous single mouse knockout studies have indicated that the loss of *Tfap2a* has the most significant effect on craniofacial development with most of the upper face absent as well as split mandible and tongue (Schorle, Meier, Buchert, Jaenisch, & Mitchell, 1996; Zhang et al., 1996). *Tfap2b* knockouts do not have gross morphological defects associated with craniofacial development (Hong et

al., 2008; Moser et al., 1997; Zhao, Bosserhoff, Buettner, & Moser, 2011), nor do pertinent knockouts of any of the three other AP-2 genes (Feng, Simoes-de-Souza, Finger, Restrepo, & Williams, 2009; Guttormsen et al., 2008; Hesse et al., 2011). We have further investigated the tissue specific requirements for *Tfap2a* in face formation and determined that its loss in the neural crest resulted in cleft palate, but otherwise only minor defects in the development of the facial skeleton (Brewer, Feng, Huang, Sullivan, & Williams, 2004). Next, we investigated whether the co-expression of *Tfap2b* might compensate for the loss of *Tfap2a* alone by deriving mice lacking both genes in NCCs. Although these NCC double knockout mice had more severe craniofacial defects, including a split upper face and mandible, the phenotype was still less severe that observed with the complete loss of *Tfap2a* alone (Van Otterloo et al., 2018; Zhang et al., 1996). In contrast, targeting *Tfap2a* in the surface ectoderm in the region of the face associated with the lens placode causes a mild form of orofacial clefting (Pontoriero et al., 2008). These findings suggested that the ectoderm may be an additional major site of *Tfap2a* action during mouse facial development, and by analogy with the NCC studies, that the phenotype could be exacerbated by the additional loss of *Tfap2b*.

Therefore, here we have assessed how craniofacial development is affected upon simultaneous removal of *Tfap2a* and *Tfap2b* in the embryonic ectoderm using the Cre transgene, *Crect*, which is expressed from E8.5 onwards throughout this tissue layer. Our results show that the expression of these two AP-2 proteins in the ectoderm has a profound effect on the underlying NCC-derived craniofacial skeleton and strengthens the association between the AP-2 family and ectodermal development and function. Furthermore, we examined how the loss of these two AP-2 transcription factors impacted the ectodermal craniofacial gene regulatory network by studying changes in chromatin accessibility and gene expression between control and mutant mice. These studies reveal critical targets of AP-2 within the facial ectoderm, especially Wnt pathway genes, and further indicate the necessity of appropriate ectodermal:mesenchymal communication for growth, morphogenesis and patterning of the vertebrate face.

RESULTS:

Combined loss of Tfap2a and Tfap2b in the embryonic surface ectoderm causes major craniofacial defects

To probe the role of AP-2 in the ectoderm during mouse facial development, we first documented expression of the five family members in the facial prominences from previous RNAseq datasets spanning E10.5 and E12.5 (Hooper et al., 2020). *Tfap2a* and *Tfap2b* were the most highly expressed, with lower levels of *Tfap2c*, and undetectable levels of *Tfap2d* and *Tfap2e* (Figure 1A). The relative abundance of the various *Tfap2* transcripts in the surface ectoderm resembles the distribution of the expression of these genes in the underlying neural crest, where *Tfap2a* and *Tfap2b* had overlapping functions in regulating facial development (Van Otterloo et al., 2018). Therefore, we next tested whether these two genes performed similar joint functions in the surface ectoderm in controlling growth and patterning. Here the Cre recombinase transgene *Crect* (Schock et al., 2017) was used in concert with floxed versions of *Tfap2a* (Brewer et al., 2004) and *Tfap2b* (Van Otterloo et al., 2018) to remove these two transcription factors (TFs) from the early ectoderm . Using scanning electron microscopy we found that at E11.5 both control and mutant embryos – hereafter designated ectoderm double knockout (EDKO) - had a similar overall facial organization, with distinct paired mandibular, maxillary, lateral and medial nasal processes (Figure 1B-E). However, there were also clear changes in the size and shape of these processes in the EDKO. The mandible was smaller with a more noticeable notch at the midline while in the upper face the maxilla and nasal processes had not come together to form a three-way lambdoid junction, and the nasal pit was more pronounced. By E13.5 these earlier morphological changes in the EDKOs were greatly exacerbated typified by a fully cleft mandible, and a failure of the MxP, LNP, and MNP to undergo any productive fusion (Figure 1F-I). These observations indicate that the AP-2 TFs, particularly AP-2α and AP-2β, are critical components of a craniofacial ectodermal gene regulatory network (GRN). In the next section we analyze this GRN in more detail, prior to describing additional analysis of the EDKO mouse model at later time points.

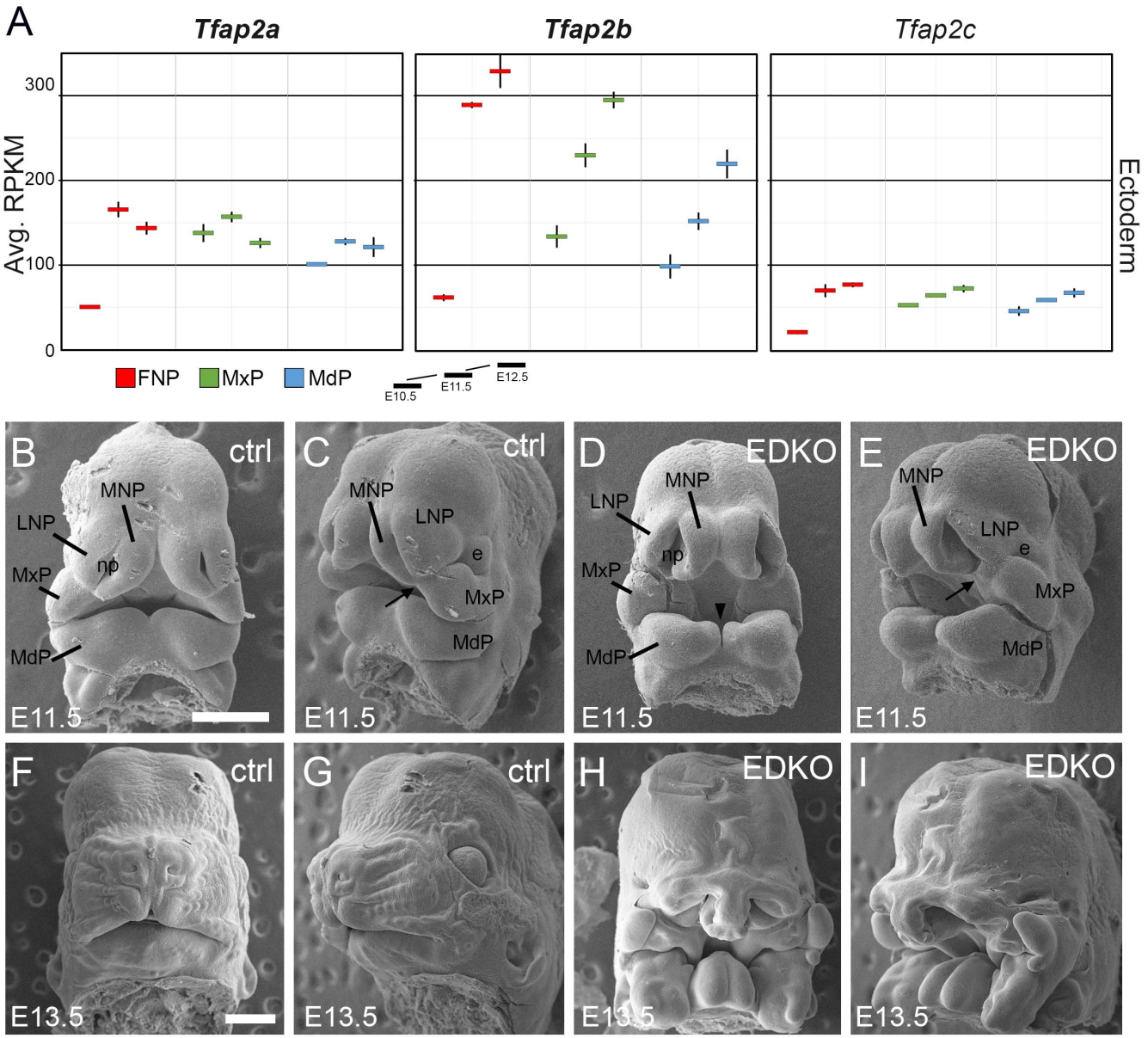

Figure 1. Expression and function of Tfap2a and Tfap2b in embryonic mouse facial ectoderm. (**A**) Chart depicting *Tfap2a*, *Tfap2b*, and *Tfap2c* expression in the three regions of the mouse ectoderm between E10.5-E12.5 (data adapted from (Hooper et al., 2020)). The lines represent the standard deviation between 3 biological replicates. (**B-I**) Scanning electron microscope images of E11.5 (B-E), or E13.5 (F-I) control (B, C, F, G) or EDKO (D, E, H, I) heads shown in frontal (B, D, F, H) and angled (C, E, G, I) view. Abbreviations: e, eye; FNP, combined nasal prominences; LNP, lateral nasal process; MdP, mandibular prominence; MNP, medial nasal process; MxP, maxillary prominence; np, nasal pit. Arrow shows position of lambdoid junction; arrowhead shows medial cleft between mandibular prominences in EDKO mutant. Scale bar = 500μm.

ATAC-seq of control and AP-2 mutant mouse craniofacial ectoderm identifies a core subset of

unique nucleosome free regions, many of which are AP-2 dependent.

To investigate this GRN—and AP-2's potential role within it—we implemented ATAC-seq (Buenrostro, Giresi, Zaba, Chang, & Greenleaf, 2013; Buenrostro, Wu, Chang, & Greenleaf, 2015; Corces et al., 2017) on surface ectoderm pooled from the facial prominences of E11.5 control or EDKO embryos, processing two biological replicates of each (Figure 2A). We choose E11.5 for analysis since at this timepoint differences in craniofacial morphology between controls and mutants were becoming evident but were not yet severe (Figure 1B-E). To assess open chromatin associated with the craniofacial ectoderm GRN, we first focused our analysis on the control ectoderm datasets. From the combined control replicates, ~65K (65,467) 'peaks' were identified above background (Figure 2B) representing open chromatin associated with diverse genomic *cis*-acting elements including promoters and enhancers. These elements were further parsed using ChIP-Seq data from E10.5 and E11.5 craniofacial surface ectoderm obtained using an antibody detecting the active promoter histone mark, H3K4me3. Specifically, the ATAC-seq peaks were classified into two distinct clusters, either high (N = 10,363) or little to no (N = 54,935) H3K4me3 enrichment (Figure 2B). Assessing the location of these peak classes relative to the transcriptional start site of genes clearly delineated them into either proximal promoter or more distal elements, respectively (Figure 2C). Motif enrichment analysis for the proximal promoter elements (Andersson & Sandelin, 2020) identified binding sites for Ronin, SP1, and ETS-domain TFs (Figure 2D, top panel, Figure S1). Conversely, the top four significantly enriched motif families in distal elements were CTCF/BORIS, p53/63/73, TEAD, and AP-2 TFs (Figure 2D, bottom panel, Figure S2). The most significant motif, CTCF/BORIS, is known to be found at insulator elements and is important in establishing topologically associated domains (J. R. Dixon et al., 2012; Ong & Corces, 2014). Notably, p53/63/73, TEAD and AP-2 family members are highly enriched in open chromatin regions associated with early embryonic skin (Fan et al., 2018) and are known to be involved in skin development and often craniofacial morphogenesis (Wang et al., 2006; Wang, Pasolli, Williams, & Fuchs, 2008; Yuan et al., 2020). Finally, pathway analysis of genes associated with either H3K4me3+ (Figure S3) or H3K4me3- (Figure S4) elements identified clear biological differences between these two subsets, with craniofacial and epithelial categories being prominent only in the latter.

We next reasoned that the H3K4me3- distal peaks likely represented regions of open chromatin

that were found in multiple tissue-types as well as some that were ectoderm-specific. Therefore, we utilized publicly available ATAC-seq datasets (Consortium, 2012; Davis et al., 2018) from additional mouse embryonic tissues (liver, kidney, intestine, brain, etc.) and plotted relative peak intensities on top of our ~55K distal peaks in the craniofacial surface ectoderm. K-means clustering of this overlap identified three distinct groups: 'tissue generic' (termed C1, N = 9,244); 'ectoderm favored' (chromatin open in surface ectoderm, but also at low levels in other tissues, termed C2, N = 24,805); and 'ectoderm unique' (termed C3, N = 20,886) (Figure 2E). Motif analyses of these three subgroups showed that C1 was most highly enriched for the CTCF/BORIS motif (Figure 2F, Figure S5) and genes nearby these elements had less relevant ectodermal/craniofacial associations (Figure S6). Conversely, C3 elements contained the p53/p63/p73, AP-2, and TEAD motifs (Figure S7), and nearby genes were highly enriched for networks associated with ectodermal and craniofacial development (Figure 2F, Figure S8). In addition, the GRHL and PBX motifs—both key TF families in surface ectoderm gene networks (Ferretti et al., 2011; Ting et al., 2005)—were the next identified within the C3 element list at high significance. The C2 list contained a mix of both C3 and C1 motifs (Figure S9) and gene network associations (Figure S10).

Next, we employed the corresponding E11.5 gene expression profiles of the mouse craniofacial ectoderm and mesenchyme (Hooper et al., 2020) and correlated the relative expression between these two tissue layers with the list of E11.5 genomic elements and associated genes identified using ATAC-seq. Genes from the expression analysis were first binned into groups (Table S1) based upon whether they had: no associated peaks; peaks associated only with C1 (tissue generic), C2 (ectoderm favored), or C3 (ectoderm unique); or peaks in multiple categories (e.g., C1+C2). We then used a cumulative distribution plot to assess the difference in distribution of 'ectoderm expression enrichment' between each group. This analysis identified that genes associated with both a C2 and C3 element showed a shift in distribution favoring ectoderm enrichment relative to genes with no associated element ($p < 2.2e-16$) (Figure 2G). In addition, if genes were also binned based on the sum of associated C2 and C3 elements, genes with 4 or greater elements, compared to those with less than 4, showed the most significant shift in distribution relative to genes with no elements (Figure S11). Collectively, these analyses identified the position of key genomic elements in the mammalian craniofacial surface ectoderm, their predicted TF

binding profiles, and correlation with ectoderm specific gene expression patterns and pathways.

Moreover, these data suggested that AP-2 binding sites within promoter distal elements of ectodermally expressed genes may play an important role in the associated GRN required for facial development.

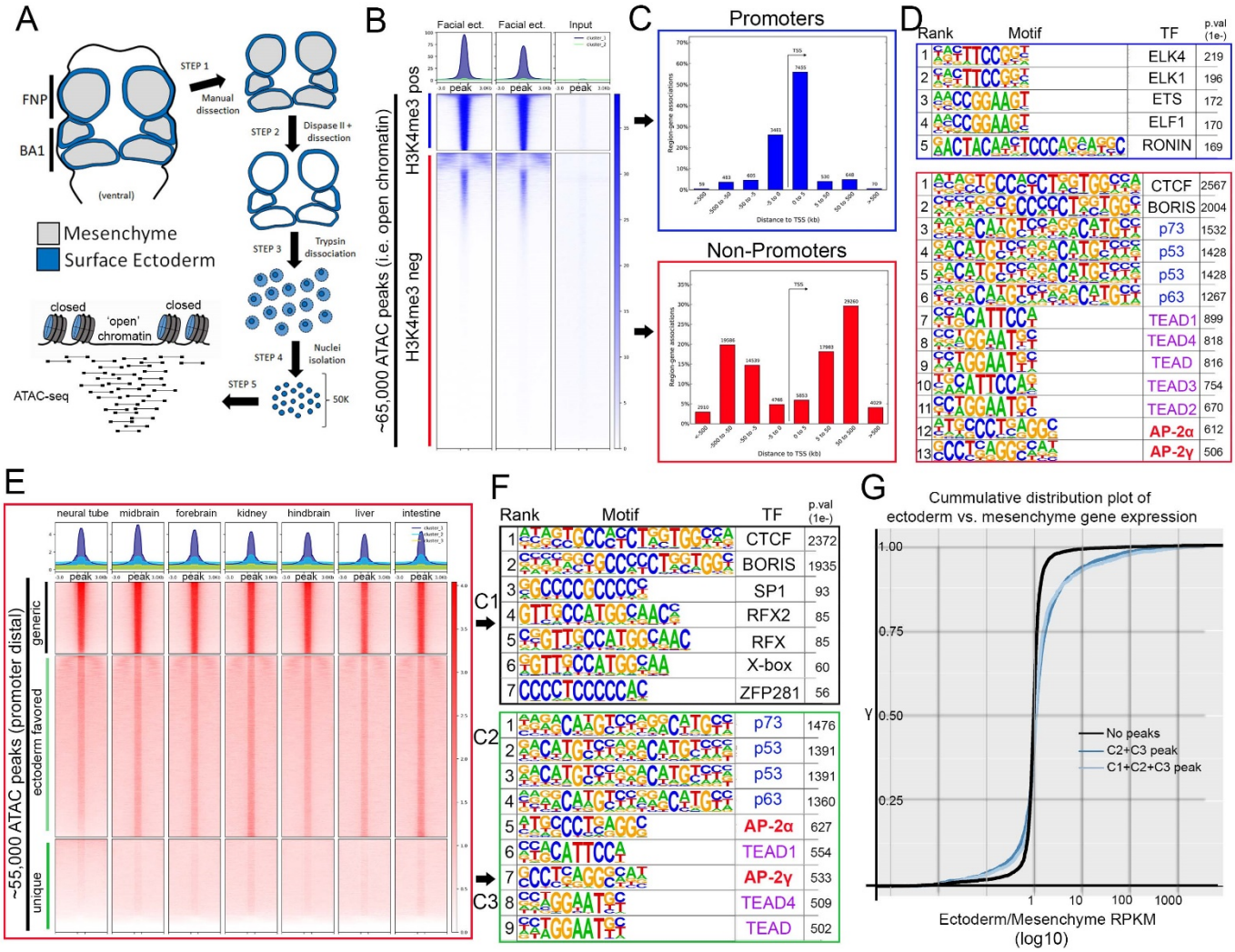

Figure 2. ATAC-seq of control E11.5 craniofacial surface ectoderm reveals nucleosome free regions. (**A**) A schematic outlining the general workflow of craniofacial surface ectoderm isolation and subsequent ATAC-seq to identify open chromatin regions. (**B**) Density plot of ~65,000 open chromatin regions identified in the control surface ectoderm (Y-axis), +/- 3 Kb (X-axis), overlaid with the H3K4me3 promoter mark from similar tissue at E10.5 (column 1), E11.5 (column 2), or non-enriched input control (column 3). (**C**) Distribution, relative to the transcriptional start site (TSS, arrow) of the elements subset in (B). (**D**) Transcription factor motif enrichment analysis of the 2 subset clusters identified in (B). (**E**) Density plot of ~55,000 non-promoter, open chromatin regions [bottom cluster in (B) replotted on Y-axis], +/- 3 Kb (X-axis) overlaid with ENCODE ATAC-seq datasets from various mouse embryonic tissues/organs. (**F**) Transcription factor motif enrichment analysis of 2 (C1 and C3) of the 3

subset clusters identified in (E) (C2 not shown). (**G**) A cumulative distribution plot of gene expression in craniofacial surface ectoderm versus mesenchyme. The groups of genes include those with no peaks (black line), those with C1, C2, and C3 peaks (light blue line), and those with C2 and C3 peaks only (dark blue line)—with 'peaks' being those defined by subclusters in (E).

Simultaneous loss of *Tfap2a* and *Tfap2b* within the surface ectoderm results in reduced chromatin accessibility at a subset of elements, including those associated with WNT ligands.

To examine how loss of *Tfap2a* and *Tfap2b* impacted chromatin accessibility in the craniofacial ectoderm, we next analyzed the ATAC-seq data from the EDKO samples and compared the results to those obtained from controls. Combined analysis of the two EDKO samples yielded ~63,000 'peaks' with CTCF, P53/P63/P73, and TEAD again the top motifs identified (Figure S12). In stark contrast to controls though, AP-2 consensus motifs were not detected, consistent with the loss of elements directly bound by AP-2 in EDKO mutants. Further, these data suggest that the limited expression of AP-2γ/*Tfap2c* in the ectoderm is not sufficient to compensate for the loss of AP-2α and AP-2β. Next, using the mutant dataset as 'background' to remove regions with similar chromatin accessibility from the control dataset, we identified genomic loci where accessibility was significantly higher in controls relative to in EDKO mutants. This differential analysis identified ~3.1K genomic regions (N = 3,103, ~5% of control elements) that were significantly decreased in accessibility upon loss of AP-2α/AP-2β (Figure 3A). AP-2 elements were the top two binding motifs in these 3.1K peaks, consistent with AP-2 directly binding many of these elements (Figure 3B, Figure S13). A more limited enrichment for p53/63/73, TEAD, and PBX motifs was also observed in these 3.1K peaks, potentially indicating that AP-2 either facilitates access of these other TFs at certain sites or simply reflecting the prevalence of these additional motifs in ectodermal control elements (Figure 3B, Figure S13).

Examination of this core subset of AP-2 dependent nucleosome free regions in the craniofacial ectoderm revealed that they are mostly promoter distal (~87%), consistent with enhancers (Figure 3C). Most genes (2432) had only one assigned peak (Table S2), but many had two (654), three (232), four (108), or five (32) peaks. Notably, 45 genes had 6 or more assigned peaks, and ~120 peaks were assigned to only four gene pairs: *Rhou/Gas8*, *Ezh2/Pdia4*, *Atg7/Hrh1*, and *Asmt/Mid1*. However, these highly clustered assignments of 20-56 peaks per gene pair represent binding to direct repeat sequences,

which skews functional annotations assigned by GREAT (Figure 3D and Figure S14). Nevertheless, multiple genes and annotations associated with development of the skin and its appendages are still present (Table S2 and Figure S14). Thus, AP-2 dependent peaks had annotations including *anchoring junction* and *adherens junction* and were associated with genes encoding keratins, cadherins, and gap junction components (Figure 3D). Similarly, GO 'Molecular Function' annotations included both *frizzled binding* and *beta-catenin binding*, and multiple Wnt pathway genes were also assigned to peaks (Figure 3D: *Wnt2b*, *Wnt3*, *Wnt3a*, *Wnt4*, *Wnt6*, *Wnt8b*, *Wnt9b*, *Wnt10a*, and *Wnt10b*)—some of which are known to be essential for proper craniofacial development (Chiquet et al., 2008; Menezes et al., 2010; Reynolds et al., 2019; Watanabe et al., 2006).

Next, we further subdivided the AP-2 dependent elements based on their overall degree of conservation across vertebrate lineages (60-way phast-con score), creating two distinct clusters, 'ultra-conserved' (N = 787 elements) and less conserved (N = 2,312 elements) (Figure 3E, F). Pathway analysis of genes associated with the ultra-conserved elements now revealed *frizzled binding* as the top 'Molecular Function'—in part, because of ultra-conserved elements near *Wnt3*, *Wnt9b*, *Wnt10a*, and *Wnt10b* (Figure 3G and Figure S15). Interestingly, the only 'Human Phenotype' listed in the non-ultra-conserved group was "*cleft lip*", in part because of elements near the *Irf6* and *Grhl3* loci, but no WNT-related categories were identified in this list (Figure S16). These findings suggest that distinct 'ancient' and 'derived' AP-2 networks exist in the craniofacial surface ectoderm. Finally, we utilized the control dataset as 'background' to look for enrichment in the EDKO dataset. This approach identified ~1.5K regions that became more accessible upon loss of *Tfap2a* and *Tfap2b*, but motif analysis of these elements did not identify an enrichment of the AP-2 binding site, suggesting that direct AP-2 DNA binding is not responsible for blocking these sites in control ectoderm (Figure S17).

In summary, our analysis of chromatin accessibility in AP-2 mutant craniofacial surface ectoderm suggests that: 1) a subset of distal nucleosome-free regions—presumed enhancers—is AP-2 dependent; 2) these elements are significantly enriched near genes regulating craniofacial and ectodermal development; 3) elements near WNT-related loci are disproportionally impacted upon loss of AP-2; and, 4) AP-2 regulation of chromatin dynamics near WNT-loci is likely a highly conserved function.

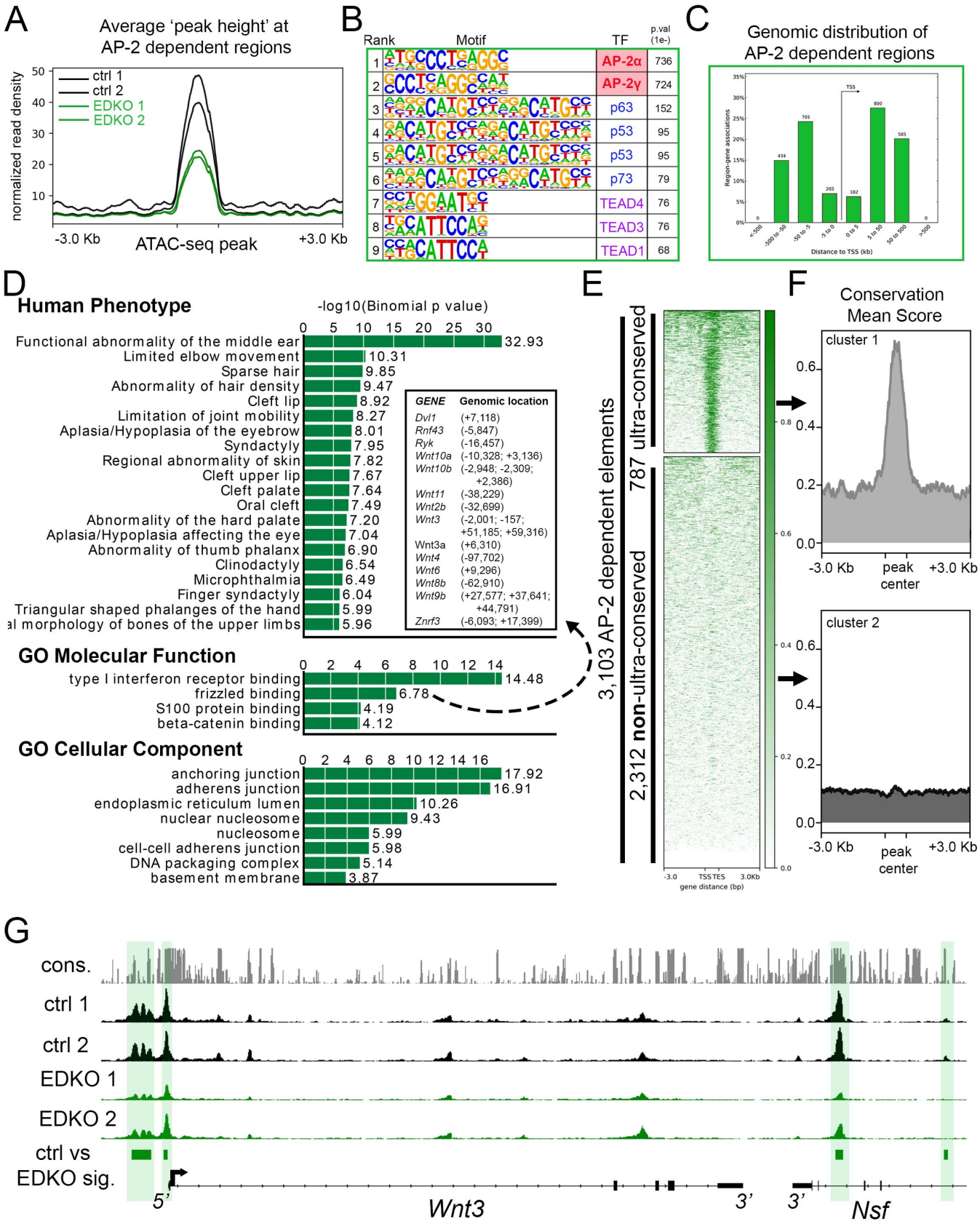

Figure 3. ATAC-seq analysis of EDKO mutants reveals AP-2 craniofacial surface ectoderm dependent nucleosome free regions. (**A**) Average normalized read density for control (black lines) and Tfap2a/Tfap2b ectoderm mutant (green lines) ATAC-seq datasets at 'AP-2 dependent' nucleosome free regions (+/- 3.0 Kb). (**B**) Transcription factor motif enrichment analysis of AP-2 dependent nucleosome free regions. (**C**) Distribution, relative to the transcriptional start site (TSS, arrow) of AP-2 dependent nucleosome free regions. (**D**) GO/pathway enrichment analysis, using GREAT, of genes located near AP-2 dependent nucleosome free regions. Note, the inset highlights the genes associated with the GO Molecular Function annotation 'frizzled binding' and the genomic location (relative to the TSS) of the associated AP-2 dependent nucleosome free region. (**E**) Density plot of ~3,100 AP-2 dependent elements (Y-axis), +/- 3 Kb (X-axis) overlaid with conservation score (e.g. darker green = more conserved) identifies 'ultra-conserved' and 'non-ultra-conserved' subclusters. (**F**) Mean conservation score of elements identified in each subcluster in (E). (**G**) IGV browser view of tracks at the *Wnt3* locus. Tracks for conservation (grey, labeled *cons.*), control ATAC-seq replicates (black, labeled ctrl 1 and ctrl 2), AP-2 mutant ATAC-seq replicates (green, labeled EDKO1 and EDKO2), and coordinates of significantly altered elements between control and AP-2 mutant datasets (green bars, labeled ctrl vs EDKO sig.). The *Wnt3* transcription unit is schematized at the bottom, along with the 3' exons of the flanking *Nsf* gene, representing ~60kb of genomic DNA.

Reduced chromatin accessibility at WNT-related genes correlates with reduced gene expression at E11.5 in *EDKO* surface ectoderm

Analysis of chromatin accessibility in EDKO mutants and controls indicated that loss of AP-2 in the ectoderm may impact expression of several genes in the WNT pathway. This was further investigated using both real-time RT-PCR and RNA *in situ* hybridization to compare expression of several members of this pathway in E11.5 embryos between control and EDKO mutants. To extend the analysis, gene expression was also analyzed in embryos with additional *Tfap2a/Tfap2b*^{Crect} allelic combinations, specifically those lacking both copies of *Tfap2a*, but still containing one functional allele of *Tfap2b* (EAKO), and those with one functional allele of *Tfap2a*, but no *Tfap2b* (EBKO). In situ hybridization for *Wnt3* and *Wnt9b* in control embryos demonstrated strong expression in the facial ectoderm, typified by the signal observed at the margins of the MxP (Figure 4A, E). This staining was absent in the *EDKO* mutants (Figure 4C, G), and the *EAKO* mutants showed an intermediate level of staining (Figure 4B, F). RT-PCR analysis of E11.5 whole facial tissue confirmed these *in situ* findings for the ectodermally-expressed ligands *Wnt3*, *Wnt9b*, as well as *Wnt10b* (Figure 4D, H, I). RT-PCR also

revealed a graded reduction in expression from control, to *EAKO*, and finally *EDKO* mutants, for these three genes but no significant loss of expression in EBKO mutants, where an intact allele of *Tfap2a* was still present. Several WNT-signaling repressors—for example, *Axin2*, *Dkk4*, and *Sostdc1*—were also associated with elements showing reduced chromatin accessibility in facial ectoderm of EDKO mutants (Figure 4M and Figure S18, S19). RT-PCR analysis of these 3 genes also showed reduced expression, especially between control and *EDKO* mutants (Figure 4J-L). Since *Axin2* has similar expression in ectoderm and mesenchyme (Leach et al., 2017) we next used RT-PCR to examine *Axin2* expression in the separated tissue layers of control and EDKO samples, in comparison to *Wnt3*, which exhibits mainly ectodermal expression (Fig S20). These studies showed that *Wnt3* down-regulation was confined to ectoderm, whereas *Axin2* expression was reduced in both tissues, suggesting that AP-2 loss in the ectoderm may also be indirectly affecting the mesenchyme gene expression program. We further examined the impact of changes in epithelial:mesenchymal interactions caused by loss of *Tfap2a/Tfap2b* in the ectoderm by studying cell proliferation in the facial prominences of E11.5 control and EDKO embryos. As shown in Figure S21, α-phospho-Histone H3 (αPHH3) immuno-fluorescence analysis revealed significant reduction in global αPHH3+ cells in mutant versus control embryos. Collectively, these analyses identify a dramatic impact of ectodermal loss of AP-2α and AP-2β on chromatin accessibility and gene expression of major WNT-signaling components. These changes in the ectoderm correlate with reduced proliferation of the underlying mesenchyme. In addition, these findings highlight a graded response caused by loss of three or more *Tfap2* alleles within the ectoderm with the presence of one functional allele of *Tfap2a* enabling some expression of critical regulatory genes, but that loss of all four *Tfap2a/b* alleles resulting in more drastic reductions.

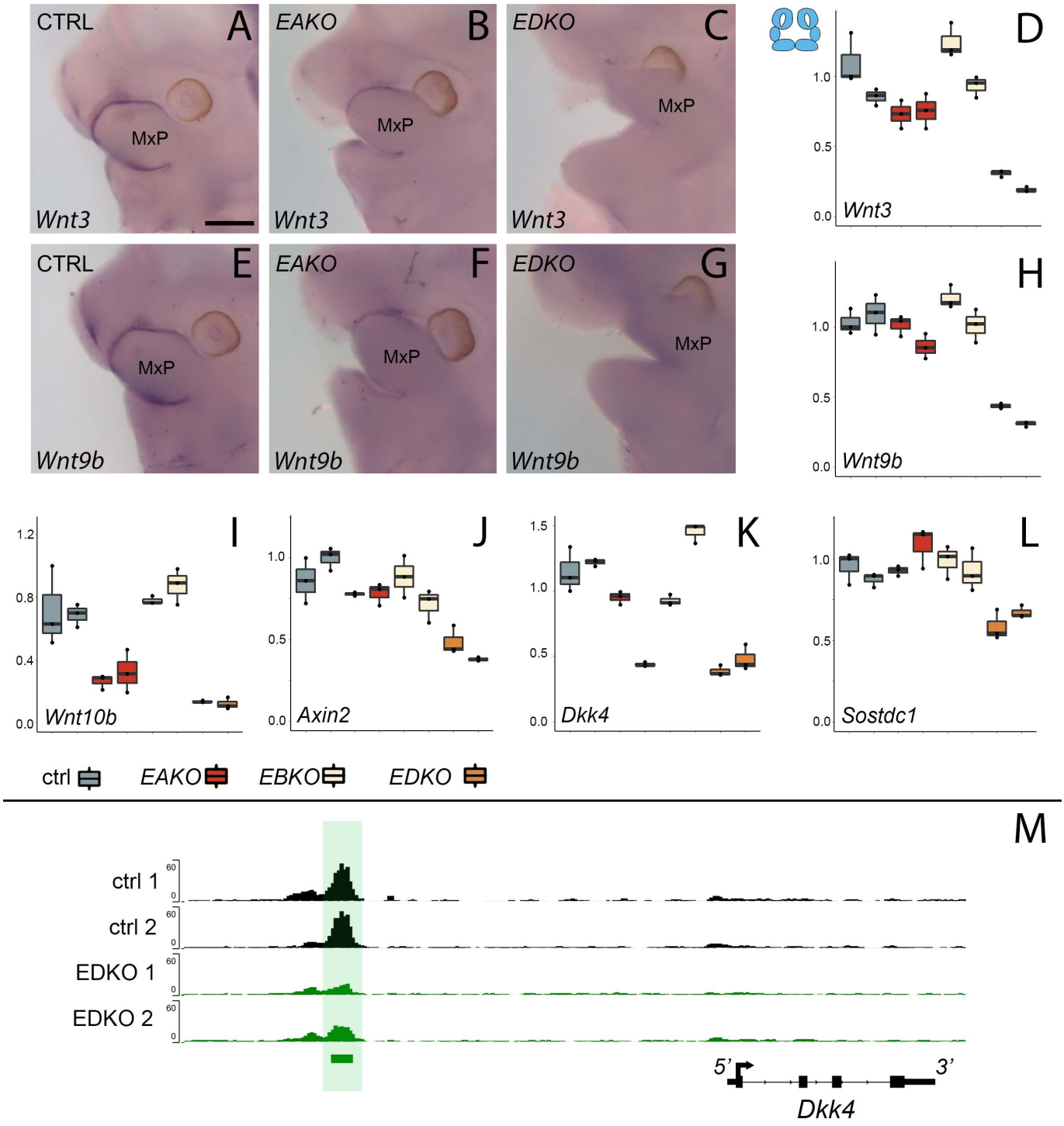

Figure 4. WNT-pathway related gene expression changes at E11.5 correlate with Tfap2 gene dosage. (A-D). Analysis of *Wnt3* expression. (**A-C**) Lateral facial views of whole mount in situ hybridization analyses of E11.5 control (**A**), EAKO (**B**), and EDKO (**C**) embryos stained for *Wnt3*. (**D**) Quantitative RT-PCR analysis of *Wnt3* expression for biological duplicates of control (grey), EAKO (red), or EBKO (yellow) and EDKO (orange) samples. The boxplots represent technical triplicates, including upper, lower, and median values. Note, RNA was derived from whole facial prominences i.e. ectoderm and mesenchyme, as shown in schematic at top left of (D). (**E-H**) Panels show equivalent whole mount and qRT-PCR analyses to (A-D) for *Wnt9b* expression. (**I-L**) Quantitative RT-

PCR analysis for *Wnt10b* (**I**), *Axin2* (**J**), *Dkk4* (**K**) and *Sostdc1* (**L**) as in panel (D). (**M**) IGV screenshot showing tracks for ATAC-seq analysis in control (top two tracks, black, ctrl 1 and ctrl 2) or EDKO (bottom two tracks, green, EDKO 1 and EDKO 2), and regions of significant difference between the two genotypes (green bar). An 'AP-2 dependent' nucleosome free region is highlighted in green ~ 6kb upstream of the 4kb mouse *Dkk4* transcription unit. MxP, maxillary prominence. Scale bar = 500 μM.

A graded response in gross craniofacial development results from different *Tfap2a* and *Tfap2b* allelic combinations in the surface ectoderm.

The graded changes in Wnt pathway gene expression observed at E11.5 EBKO, EAKO, and EDKO embryos suggested that the loss of different allelic combinations of *Tfap2a* and *Tfap2b* in the facial ectoderm might also have functional consequences for facial development. After determining that certain allelic combinations did not survive postnatally, we found that at E18.5, EBKO embryos (Figure 5C, C'), were indistinguishable from controls (Figure 5A, A') whereas *EAKO* (Figure 5B, B') and *EDKO* (Figure 5D, D') embryos displayed substantial defects. *EAKO* embryos exhibited bilateral facial clefting, a cleft palate, a cleft hypoplastic mandible, bifid tongue, hypoplastic and low-set pinna, and a partial ventral body-wall closure defect (Figure 5B, B'). These phenotypes were exacerbated in *EDKO* embryos, with most craniofacial structures severely malformed (Figure 5D, D'), displaying a complete failure of the facial prominences to grow towards the midline, with the maxilla and mandible growing out laterally from the oral cavity, resulting in a mandibular and palatal cleft, consistent with the morphological defects observed at earlier time points (Figure 1). Similarly, structures derived from the MNP and LNP failed to fuse with each other or the maxilla, instead growing dorsally, resulting in exposure of the developing nasal cavity (Figure 5D, D'). External pinnae were notably absent and there was also microphthalmia (Figure 5D, D'). Compared to the EAKO mutants, EDKO embryos also had a more severe ventral body wall closure defect, with an open thorax (Figure 5D'). A small percentage of *EDKO* mutants also had a failure of dorsal neural tube closure, resulting in exencephaly (data not shown). Finally, *EDKO* mutants also displayed an apparent thinning of the epidermal layer, resulting in tissue transparency, most obvious around the lateral portions of the neck (Figure 5D). Collectively, these findings reveal that functional redundancy exists between AP-2α and AP-2β within the ectoderm lineage—most notably in the context of facial morphogenesis. Furthermore, these results indicate that AP-2α has the most potent TF activity

since mice lacking *Tfap2b*, but containing one functional copy of *Tfap2a*, can still undergo normal facial development, whereas the reverse results in orofacial clefting.

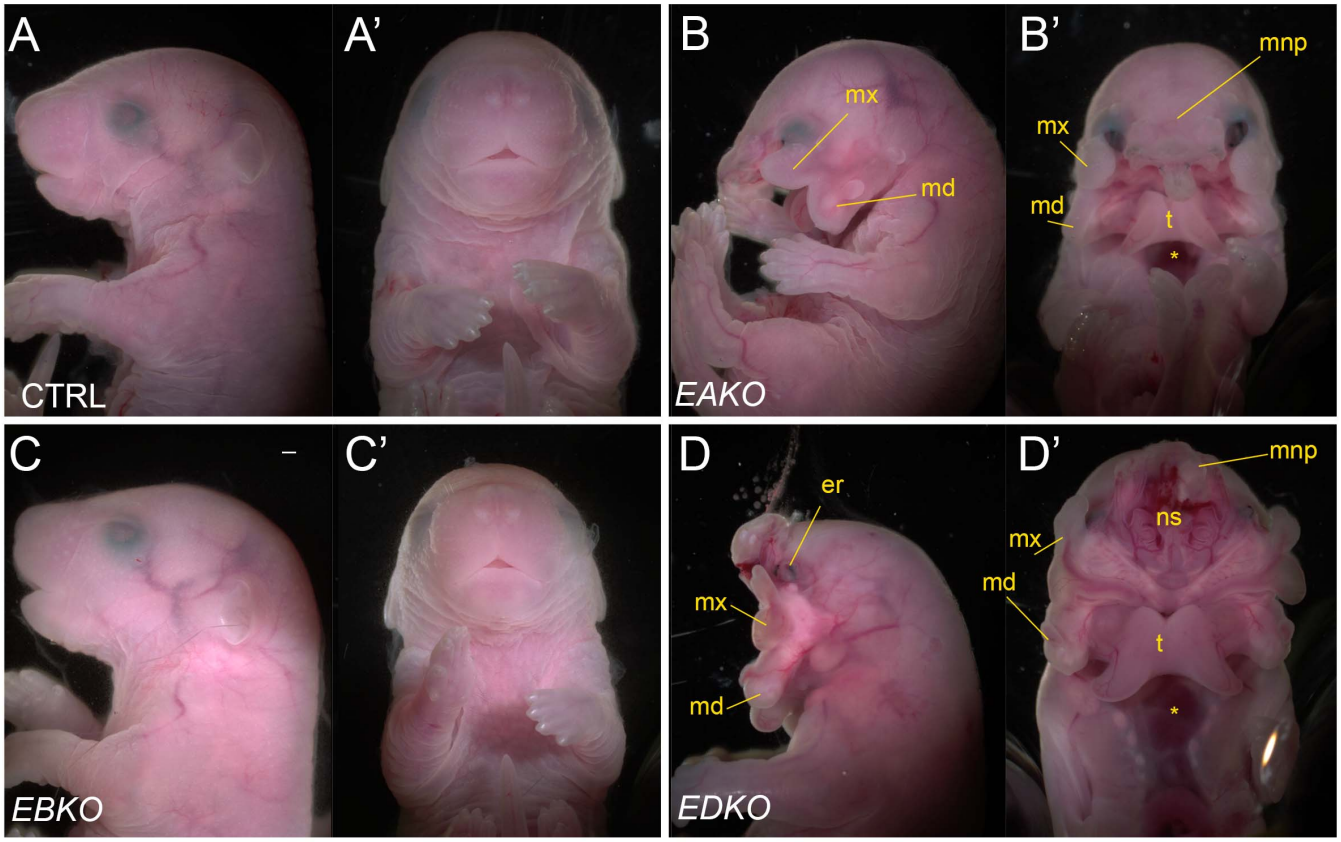

Figure 5. Gross morphological phenotypes of E18.5 control, EAKO, EBKO, and EDKO mutants. Lateral (**A-D**) or ventral (**A'-D'**) views of an E18.5 control (A, A'), EAKO (B, B'), EBKO (C, C'), or EDKO (D, D') embryo. Abbreviations: md, mandible; mnp, medial nasal prominence; mx, maxillary prominence; er, eye remnant; ns, nasal septum; t, tongue. Asterisks in B' and D' indicates ventral body wall closure defect. Scale bar = 500 μM.

Disruption of neural crest derived craniofacial bone and cartilage elements in *EDKO* mutants.

To further assess the effect of loss of *Tfap2a* and *Tfap2b* within the facial ectoderm, E18.5 embryos were processed by alizarin red and alcian blue staining, revealing bone and cartilage elements, respectively (Figure 6). The craniofacial skeleton can be grouped into three structural units: the viscerocranium (comprising solely NCC derived facial elements); neurocranium (calvaria/skull vault); and chondrocranium—the latter two units having both a NCC and mesoderm origin [reviewed in (Minoux & Rijli, 2010)]. Control and *EBKO* embryos displayed the typical NC-derived craniofacial elements (Figure 6A, D, G, J,) whereas both *EAKO* and *EDKO* embryos demonstrated major disruption to several of these

skeletal structures. First, in *EAKO* skeletons (Figure 6B, E, H, K), the most substantially affected structures included a shortened, cleft mandible, hypoplastic development of the maxillary, nasal, lamina obturans and palatine bones (consistent with the bilateral facial clefts and clefting of the secondary palate), a slightly hypoplastic frontal bone, and missing tympanic bones. The premaxillary bone developed anteriorly into a long bony element protruding at the front of the face, presumably due to the absence of constraints imposed by fusion to the maxilla (Figure 6B)—a feature commonly observed in humans with orofacial clefting (Nyberg, Hegge, Kramer, Mahony, & Kropp, 1993). In addition, isolation of the mandible revealed disruption to the patterning of the proximal end, including the normally well-defined condyles seen in control embryos (Figure 6J, K). These defects were even more pronounced, and in some instances unique, in *EDKO* mutants. Thus, several NC derived bones that were hypoplastic in *EAKO* mutants were virtually absent in the *EDKO* mutants, including the squamosal, jugal, palatine, and lamina obturans (Figure 6C, F, I). Like *EAKO* mutants, the tympanic bones were absent, the frontal bone hypoplastic, and the premaxillary bone protruding in *EDKO* mutants, although this latter process grew mediodorsally reflecting the more extreme outward growth of the facial prominences in the latter genotype. Both the mandible and maxillary bones, comprising the lower and upper-jaw, respectively, were more severely impacted in *EDKO* mutants, including a loss of the primary and secondary jaw joints, resulting in syngnathia (Figure 6C). Like *EAKO* mutants, isolation of the mandible in *EDKO* mutants revealed a major loss of proximal condylar identity, that was exacerbated by fusion with upper-jaw components (Figure 6L). Also, in contrast to *EAKO* embryos, the oral/aboral axis of the mandible was disrupted, resulting in a less pronounced tapering at the distal end (Figure 6L). To further investigate these unique features, we subsequently stained the chondrocranium of control, *EAKO*, and *EDKO* embryos at E15.5 with alcian blue (Figure 6M-O). Notably, this analysis revealed that *EDKO* mutants displayed a duplicated Meckel's cartilage along the length of the proximal-distal axis of the mandible, a feature not observed in other genotypes, and consistent with a duplication of the mandible along the oral/aboral axis (Figure 6M-O).

In summary, skeletal analysis indicated that the NC derived elements in the craniofacial skeleton were most exquisitely sensitive to loss of AP-2α and AP-2β from the surface ectoderm. In contrast, mesoderm derived components, such as the basioccipital of the cranial base, appeared less affected in

426 *EAKO* and *EDKO* mutants (Figure 6D-F). These findings are consistent with AP-2 expression in the ectoderm affecting short range signaling to the adjacent NCC mesenchyme to control growth and

428 morphogenesis.

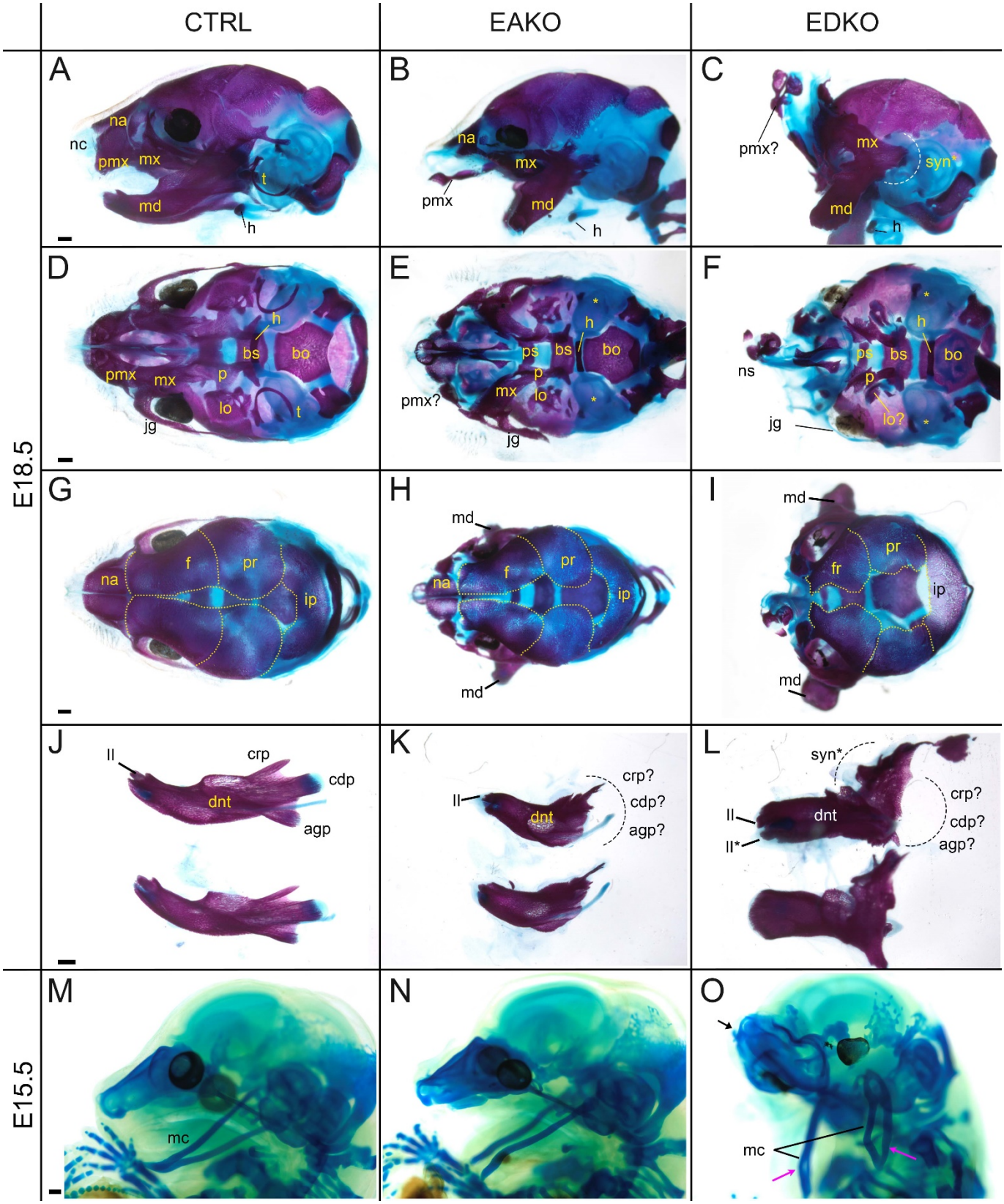

430

Figure 6. Craniofacial skeleton and chondrocranium defects vary with AP-2 gene dosage. (**A-L**) E18.5 alizarin red and alcian blue stained craniofacial elements. Lateral (**A-C**), ventral (**D-F**), dorsal (**G-I**) views of the craniofacial skeleton, and lateral views of the left and right hemi-mandibles in isolation (**J-L**) in control (**A, D, G, J**), EAKO (**B, E, H, K**), and EDKO (**C, F, I, L)** embryos. Note that the mandibles have been removed in (D-F) for clearer visualization of the cranial base, and the calvaria are outlined with yellow dashed lines in (G-I). The white dashed line in (C) highlights fusion of the upper and lower jaw (syngnathia), also indicated by the black dashed lines in (L). (**M-O**) E15.5 alcian blue stained chondrocraniums from a control (M), EAKO (N), or EDKO (O) embryo. A cleft Meckel's cartilage is highlighted by the pink arrowhead in (N) or by black lines in (O). Note, Meckel's cartilage is also duplicated (pink arrows) along the proximodistal axis of the lower jaw in (O) and upturned nasal cartilages are highlighted by the black arrow. Abbreviations: agp, angular process; bs, basisphenoid; bo, basioccipital; cdp, condylar process; crp, coronoid process; dnt, dentary; f, frontal; h, hyoid; ii, inferior incisor; ii*, duplicated incisor; ip, interparietal; jg, jugal; lo, lamina obturans; mc, Meckel's cartilage; md, mandible; mx, maxillary; na, nasal; nc, nasal cartilage; ns, nasal septum; p, palatine; pmx, premaxillary; pr, parietal; ps, presphenoid; syn*, sygnathia; t, tympanic ring; ? indicates possible identity of dysmorphic structure; * in (E, F) indicates missing tympanic ring.

RNA-seq analysis of E10.5 *EDKO* mutants reveals early disruption of WNT signaling components along with reciprocal mesenchymal perturbations.

To obtain a more global assessment of the gene expression changes in the ectoderm and how they impact the underlying mesenchyme we performed RNAseq analysis of the whole face at E10.5 for both control and EDKO mice (Figure 7A). This timepoint was chosen to detect primary changes in gene expression before major morphological differences were apparent in the mutants. Three biological replicates of each genotype were processed and the read data for each gene are summarized in Table S3. An initial assessment of the data was made by examination of a list of ~240 genes that satisfied a 1.5 fold cut-off in gene expression difference between controls and mutants, and which had consistent and measurable expression changes when viewed on the IGV browser (Table S3). This manually curated list revealed that multiple genes down-regulated in the mutant were associated with development and function of the ectoderm (Table 1). Notably, there was reduction in *Krt5*, *Krt14*, and *Krt15* expression, as well as for several genes associated with the periderm, balanced by a rise in *Krt8* and *Krt18* transcripts, indicating a delay or inhibition of normal stratification. Further, mRNAs for TFs

associated with epidermal development, particularly *Trp63*, *Grhl3* and *Foxi2*, were also reduced in the mutant. Other notable changes occur in signaling molecules associated with the WNT pathway, with Cxcl factors and to a lesser extent with genes involved in Notch, Edn, and Fgf signaling. Prominent up-regulated genes included *Lin28a* and *Cdkn1a*, which correlate with the reduced expression of genes for ectodermal differentiation and the inhibition of growth noted by more limited α-PHH3+ stained cells in the mutants (Figure S21).

Many of the genes we had identified had an ectodermal connection even though such genes are underrepresented in the analysis of whole prominence tissue. We therefore adopted a second approach to help distinguish the relevant tissue-specific expression differences. Here we focused on a group of 711 genes that satisfied a 1.2 fold-change and $Q < 0.05$ cut off between control and *EDKO* samples (Figure 7B, C, and Table S3). Of these, 365 were down-regulated and 346 upregulated, with no statistically significant difference between fold-change of up and down-regulated genes (Figure 7B, D). We next employed published gene expression levels for both the ectoderm and mesenchyme of control E10.5 wild-type embryos to distinguish the relevant tissue-specific expression differences (Hooper et al., 2020). Of the 711 genes that were differentially expressed, 438 showed > 2-fold enrichment between control tissue layers (i.e., either higher in ectoderm or higher in mesenchyme). We then used this information (Figure 7E, Y-axis), alongside the relative change in expression between controls and mutants (Figure 7E, X-axis), to stratify the differentially expressed genes into four major groups (Q1-4, Table S3). Specifically, we identified genes with preferential expression in the control ectoderm that were ‘down-regulated’ (Figure 7E, Q1, N = 103) or ‘up-regulated’ in mutants (Figure 7E, Q2, N = 171) and likewise for the mesenchyme ‘down-regulated mesenchyme’ (Figure 7E, Q3, N = 133) and ‘up-regulated mesenchyme’ (Figure 7E, Q4, N = 31). Statistical analysis of the fold-change between quadrants identified a significantly greater magnitude of fold-change in ectoderm vs. mesenchyme (Figure 7F) most likely due to down-regulated ectodermal genes (i.e. Q1) vs. all other quadrants (Figure 7G). These data suggest that, although representing a smaller fraction of the entire tissue sampled, larger changes in gene expression were within the ectoderm lineage of E10.5 mutants.

To address further how the individual genes affected in mutant vs. control embryos fit within larger biological processes and developmental systems, we utilized Enrichr (Chen et al., 2013; Kuleshov

et al., 2016) along with our stratified gene lists (Figure 7H, Table S3). First, using genes differentially expressed within the ectoderm (Q1 and Q2, N = 274) we identified the most over-represented pathway was 'WNT-signaling', which occurred in four of the top five categories (Figure 7H)—strongly supporting our ATAC-seq and targeted gene expression analysis at E11.5. In contrast, analysis of pathways over-represented in the mesenchyme differentially expressed gene list (Q3 and Q4, N = 164), identified the top pathways to include 'GPCR', 'Osteoblast', and 'Neural crest' (Figure 7H). Examination of over-represented TF binding sequences within the promoters of genes mis-regulated in the ectoderm identified *TFAP2A* as the most significant (Figure 7H). Further, we assessed how the expression data correlated with the ~3.1K AP-2 dependent promoter and enhancer peaks from the ectoderm ATAC-seq results. The Q1 genes, representing "down-regulated ectoderm" had the greatest overlap with 56/103 (~54%) genes having AP-2 dependent peaks while in contrast, Q2 had 57/171 (33%), Q3 had 30/133 (23%), and Q4 had 10/31 (32%). The higher proportion of AP-2 dependent peaks associated with Q1 strongly suggests that AP-2 directly regulates many of these genes within the facial ectoderm, including members of the Wnt pathway, Irx family, and keratins (also see Table 1). Conversely, genes mis-regulated in the mesenchyme were shown to be significantly enriched for TCF12/4/3-interactors based on protein-protein interaction databases (Figure 7H) supporting a model in which genes affected within the ectoderm are more likely direct targets of AP-2, whereas those impacted in the mesenchyme are more likely to be indirect. The ectoderm Q1/Q2 gene list also highlighted annotations for orofacial clefting (Figure 7H)—fitting with the clefting phenotype observed in mutant embryos. Included within this list were the human clefting genes, *TRP63* (Celli et al., 1999) and *GRHL3* (Leslie et al., 2016; Peyrard-Janvid et al., 2014)—both highly enriched within the ectoderm lineage and the former a proposed AP-2 transcriptional target in humans (L. Li et al., 2019)—which were significantly down-regulated within *EDKO* mutants, relative to controls (Table S3).

Finally, 32 out of the total 710 differentially expressed genes were related to the Wnt signaling pathway, (Figure 7B, Figure S22), and their average fold-change was significantly more that the average fold-change of the remaining 678 genes ($p < 0.05$) (Figure 7I). This comparison was even more significant when examining genes solely within Q1 ($p < 0.005$) (Figure 7I). That is, Wnt-pathway genes down-regulated in the ectoderm of *EDKO* mutants, relative to controls, were more significantly impacted

than all other genes represented in Q1. Numerous WNT components—many of which were previously identified from our ATAC-seq data—including ligands (*Wnt3*, *Wnt4*, *Wnt6*, *Wnt9b*, *Wnt10b*, *Wnt10a*), WNT inhibitors (*Dkk4*, *Kremen2*, *Sostdc1*), and a WNT receptor (*Fzd10*), were represented within this list (Table S3). Consistent with these genes being expressed in the ectoderm, their read-based calculated expression levels were often low relative to mesenchymal genes but showed striking congruence between triplicates (Figure 7J). We note that the reduced expression observed for several of these genes at E10.5 in the RNAseq data was also observed at E11.5 by in situ and RT-PCR analysis (Figure 4). Furthermore, we also validated the changes seen at E10.5 for *Wnt3*, *Wnt9b*, *Kremen2* and *Sostdc1* using a combination of RT-PCR and in situ analysis (Figure S23).

Although Q1 genes, assigned as ectodermal down-regulated, had the most significant changes in expression (Figure 7G), several other WNT-related genes were also impacted in *EDKO* mutants. Specifically, additional WNT modulators (mostly repressors), *Rspo2*, *Nkd2*, *Nkd1*, *Axin2*, *Dkk2*, and *Kremen1* were also significantly down-regulated in mutant embryos (Table S3). Most of these genes were expressed at relatively equal contributions in ectoderm and mesenchyme, or solely in the mesenchyme, and we speculate their down-regulation is likely the result of a negative feedback loop upon reduced expression of Wnt ligands from the ectoderm. In addition, several Wnt receptors (*Fzd5*, *Fzd8*, *Fzd9*) were up-regulated (Table S3), potentially as a response to reduced Wnt ligand levels. In summary, bioinformatic analyses of control and *EDKO* mutants identified AP-2α and AP-2β as essential, cooperative, regulators of multiple signaling pathways and processes originating from the ectoderm during craniofacial development, most notably the WNT pathway.

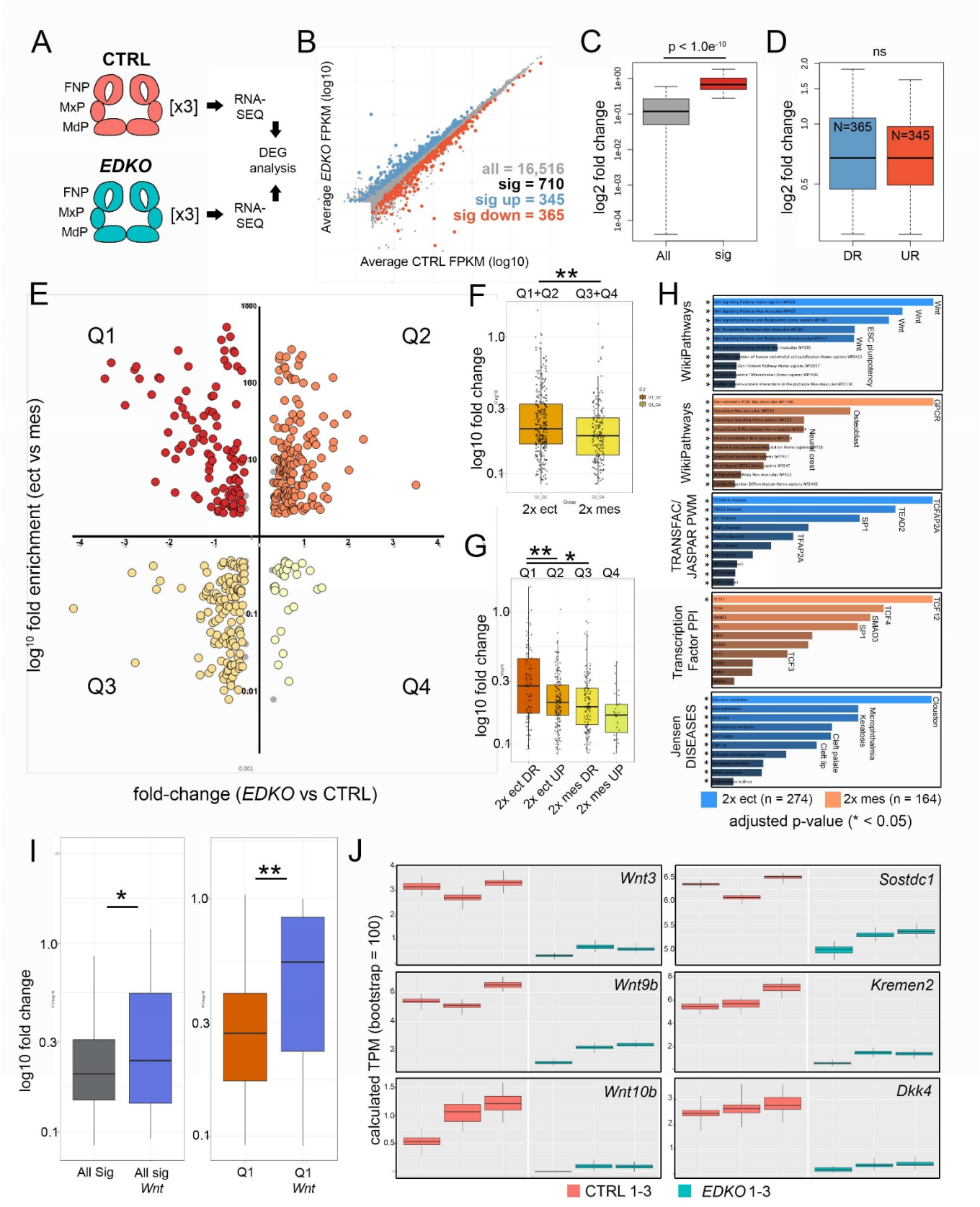

538 **Figure 7. RNA-seq analysis of E10.5 control and EDKO mutant craniofacial prominences.** (**A**) Schematic depicting regions isolated and general workflow for RNA-seq analysis. (**B**) Scatterplot of gene mean expression values (FPKM) for control (X-axis) and EDKO mutant (Y-axis) samples, blue or orange dots representing genes

significantly upregulated or downregulated in mutants versus controls, respectively. (**C**) Boxplot of mean fold-change values (mutant versus control) for all expressed genes (grey) or those that were significantly altered (red). (**D**) Boxplot of mean gene expression fold-change values (mutant versus control) for down-regulated (blue) or up-regulated (orange) genes. (**E**) Scatterplot of mean gene expression fold-change between mutant and control samples (X-axis) and mean gene expression fold-change between craniofacial ectoderm and mesenchyme (Y-axis). (**F**) Boxplot of mean gene expression fold-change values (mutant versus control) for 'ectoderm enriched' (orange) or 'mesenchyme enriched' (yellow) genes. (**G**) As in (F) but further subset into each quadrant. (**H**) Gene-set enrichment analysis (using ENRICHR) for 'AP-2 dependent' ectoderm (blue) or mesenchyme (orange) enriched genes. (**I**) Boxplots of mean gene expression fold-change values (mutant versus control) for all significantly altered genes (grey) versus those found specifically in the WNT-pathway (blue) or all significantly down-regulated ectoderm genes (Q1 genes, red) versus WNT-pathway associated genes down-regulated in the ectoderm (Q1 Wnt, blue). (**J**) RNA-seq based, computed gene expression values (TPM) for a subset of WNT-related genes, shown as biological triplicates in control (salmon) or EDKO mutant (teal). For all boxplots, the median is indicated by the horizontal line, 75th and 25th percentiles by the limits of the box, and the largest or smallest value within 1.5 times the interquartile range by the lines. A standard two-tailed t-test was conducted to calculate significance in C, D, F, G, and I (* = p-value < 0.05; ** = p-value < 0.005). Abbreviations: DEG, differentially expressed genes; DR, down-regulated; FNP, nasal processes; MdP, mandibular prominence; MxP, maxillary prominence; ns, not significant; TPM, transcripts per million; UR, up-regulated.

WNT1 over-expression partially rescues craniofacial defects in AP-2 ectoderm mutants

Axin2 is a direct target of Wnt signaling, and the *Axin2-LacZ* allele (Lustig et al., 2002) was incorporated into the *EAKO* and *EDKO* mutant backgrounds as a means to determine if the loss of AP-2 alleles in the ectoderm had a direct impact on Wnt pathway output. In E10.5 control embryos in which *Tfap2a/Tfap2b* had not had not been targeted, β-gal activity was robust within all facial prominences and the second branchial arch (Figure 8A). In contrast, *EAKO* mutants displayed a reproducible drop in β-gal staining intensity throughout these regions, with the most striking disruption around the 'hinge' (intermediate) domain of BA1 (Figure 8B). Finally, consistent with a more exacerbated phenotype and WNT pathway perturbation, *EDKO* mutants showed an even more prominent drop in β-gal staining (Figure 8C). Notably, β-gal activity was clearly reduced in mesenchymal populations, supporting a model in which ectodermal AP-2 influences ectodermal to mesenchymal WNT signaling.

We next assessed whether elevating WNT-signaling could mitigate the craniofacial defects observed in *EAKO* and *EDKO* embryos by incorporating an allele that expresses *Wnt1* upon Cre mediated recombination (Carroll, Park, Hayashi, Majumdar, & McMahon, 2005) into our *Tfap2* allelic series. In this approach, the Crect transgene both inactivates any floxed *Tfap2* alleles as well as concurrently activates *Wnt1* expression in the ectoderm (Figure 8D). Comparison of E13.5 *EAKO* to *EAKO/Wnt1*^{ox} embryos indicated that while the former (Figure 8E) had bilateral cleft lip and primary palate with a protruding central premaxilla (9 of 9), most of the latter (11/13) had achieved upper facial fusion, so that there was a slight midfacial notch in place of the aberrant premaxilla as well as the formation of nares (Figure 8F, G). Similarly, all *EDKO* mice (Figure 8H) had facial fusion defects leading to the prominent central premaxilla (9 of 9), but in *EDKO/Wnt1*^{ox} embryos (Figure 8I, J) the severity of the clefting was diminished and the central premaxilla replaced with nares (7 of 7). Note that the face was still dysmorphic in the rescued embryos, possibly reflecting insufficient Wnt pathway activity, novel defects resulting from ectopic Wnt1 expression, or additional functions regulated by AP-2 beyond the Wnt pathway. Nevertheless, these data indicate that supplementing the loss of ectodermal Wnt ligands in EAKO and EDKO mice can rescue major aspects of upper facial clefting fitting with our model that one of the main functions of these TFs is to regulate the WNT pathway.

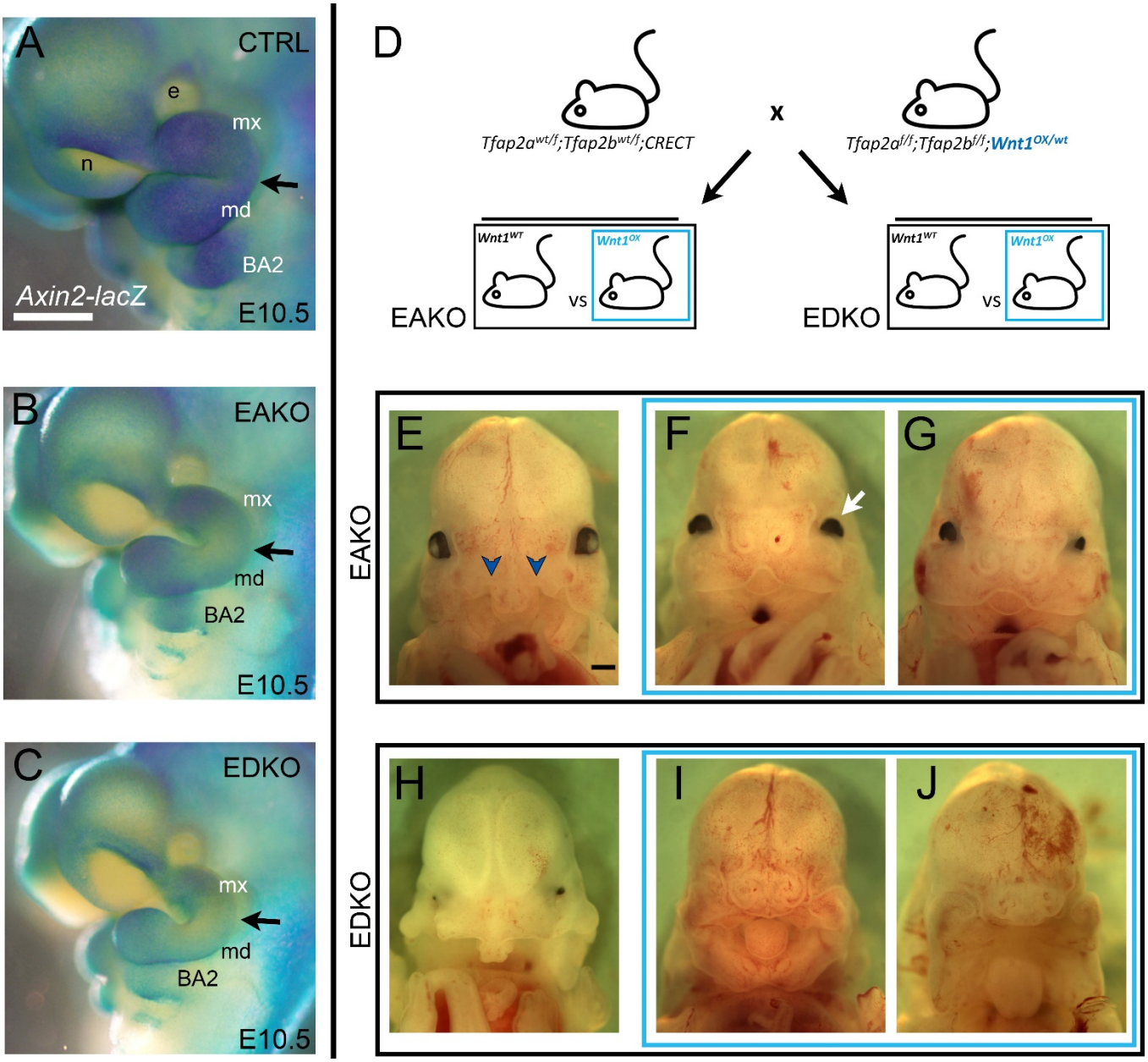

588 **Figure 8. Genetic interaction between *Tfap2* and the *Wnt* pathway.** (**A-C**) Lateral views of E10.5 β-
galactosidase stained control (A), EAKO (B) and EDKO (C) embryos harboring the *Axin2-lacZ* reporter allele. The
590 black arrow marks the position of the hinge region. (**D**) Schematic of genetic cross used to elevate Wnt1 expression
levels in control, EAKO, or EDKO mutant embryos. (**E-G**) Ventral craniofacial view of E13.5 EAKO mutants that
592 lack (E) or contain (F, G) the Wnt1 over-expression allele. The blue chevrons indicate the bilateral cleft present in
(E). The white arrow indicates the lack of lens development previously noted from an excess of Wnt signaling
594 (Smith, Miller, Song, Taketo, & Lang, 2005). (**H-J**) Ventral craniofacial view of E13.5 EDKO mutants that lack (H)
or contain (I, J) the Wnt1 over-expression allele. Abbreviations: BA2, branchial arch 2; e, eye; md, mandibular
596 prominence; mx, maxillary prominence; n, nasal pit.

598

Discussion

Development of the vertebrate head requires critical regulatory interactions between various tissue layers, particularly the ectoderm and underlying neural crest derived mesenchyme. Here we show that AP-2 transcription factors are an essential component of a mouse early embryonic ectoderm GRN directing growth and morphogenesis of the underlying facial prominence tissues. Specifically, combined conditional loss of the two most highly expressed members of the family within the ectoderm, *Tfap2a* and *Tfap2b*, results in a failure of the facial prominences to meet and fuse productively. Thus, the mandibular processes fail to meet at the midline, resulting in a wide separation between the two halves of the lower jaw, and a bifid tongue. In the upper face, the maxillary, and lateral and medial nasal prominences fail to align at the lambdoid junction, resulting in an extensive bilateral cleft and significant midfacial dysmorphology. In addition to the orofacial clefting phenotypes, there was also loss of the normal hinge region between the mandible and maxilla resulting in sygnathia, and a duplication of Meckel's cartilage. Overall, the data indicate that appropriate growth, morphogenesis, and patterning of the facial prominences are all severely disrupted. The finding that AP-2α and AP-2ß work redundantly in the facial ectoderm complements studies showing that they can also work together within the cranial neural crest to control facial development (Van Otterloo et al., 2018). In these previous studies, the neural crest specific deletion of these factors resulted in a different type of orofacial cleft – an upper midfacial cleft—but in common with the EDKO mutants also caused sygnathia. The observations that AP-2α and AP-2ß have distinct as well as overlapping functions with both the neural crest and ectoderm for mouse facial development also inform both human facial clefting genetics and evolutionary biology. With respect to humans, *TFAP2A* mutations are associated with Branchio-Oculo-Facial Syndrome (MIM, 113620), while *TFAP2B* is mutated in Char Syndrome (MIM, 169100) (Satoda et al., 2000). Although both syndromes have craniofacial components to their pathology, including changes to the nasal bridge and the position of the external ears, only mutations in *TFAP2A* are associated with orofacial clefting, usually lateral. These findings support a more significant role for *TFAP2A* in influencing orofacial clefting in both mouse and human, and suggest that it is the reduction of AP-2α function in the ectoderm—rather than the NCC—that is associated with this human birth defect.

In the context of chordate evolution, the prevailing hypothesis is that AP-2 has an 'ancestral' role

within the non-neural ectoderm followed by an 'evolved' role within the neural crest cell lineage of vertebrates (Meulemans & Bronner-Fraser, 2002; Van Otterloo et al., 2012). The current studies further support that AP-2 proteins have critical roles within the embryonic ectoderm that have been conserved from cephalochordates and tunicates through to mammals. Alongside established roles for AP-2 transcription factors in NCCs (Brewer et al., 2004; Martino et al., 2016; Prescott et al., 2015; Van Otterloo et al., 2018), these observations raise the possibility that there may be a coordinated and complex interplay between AP-2 activity in the two tissue layers that has been conserved during evolution. The combined function of the two AP-2 factors in craniofacial development also reflects the more severe pathology resulting from the loss of more than one AP-2 gene that has been documented in other mouse developmental systems including the eye, nervous system, and skin (Hicks et al., 2018; Schmidt et al., 2011; Wang et al., 2008; Zainolabidin, Kamath, Thanawalla, & Chen, 2017). The propensity of the AP-2 proteins to act in concert has also been observed in additional vertebrate species, particularly in the chick and zebrafish, where loss of more than one gene uncovers joint functions in neural crest, face, and melanocyte development (Hoffman, Javier, Campeau, Knight, & Schilling, 2007; Knight, Javidan, Zhang, Nelson, & Schilling, 2005; W. Li & Cornell, 2007; Rothstein & Simoes-Costa, 2020; Van Otterloo et al., 2010). Notably, in the zebrafish, previous studies have documented an interaction between AP-2α and AP-2ß during cranial NCC development (Knight et al., 2005). Unlike in the mouse, AP-2ß's role was confined to the surface ectoderm, based on gene expression and transplant experiments. However, more recent single-cell transcriptome profiling has identified *tfap2b* expression in the zebrafish cranial neural crest (Mitchell et al., 2021), suggesting features between these models (i.e., zebrafish and mouse) may be more conserved than previously thought.

The joint function of these AP-2 proteins in controlling specific aspects of gene expression presumably reflects the similar consensus sequence recognized by all family members (Badis et al., 2009; Bosher, Totty, Hsuan, Williams, & Hurst, 1996; Williams & Tjian, 1991). Thus, the absence of AP-2ß alone may not cause major developmental issues in mouse facial development due to the ability of the remaining AP-2α protein to bind and regulate shared critical genes. However, loss of both proteins would lower the amount of functional AP-2 protein required for normal gene regulation. The hypothesis that particular levels of AP-2 are required for achieving critical thresholds of gene activity is also

supported by the different phenotypes uncovered by the loss of particular *Tfap2a* and *Tfap2b* allelic combinations. Thus, while the loss of one allele of *Tfap2a*—or both alleles of *Tfap2b*—in the ectoderm is tolerated in the context of facial development, the combined loss of three of four *Tfap2a* and *Tfap2b* alleles is not, and the phenotypes become more severe when all four alleles are defective. We note that this phenomenon was also observed when these genes were targeted in the neural crest (Van Otterloo et al., 2018). In both the NCCs and ectoderm the role of AP-2α seemed to be more significant than AP-2ß based on the phenotypes observed—since the presence of one functional allele of *Tfap2a* resulted in less severe pathology than the converse where only a single productive *Tfap2b* allele was expressed. Currently, it remains unclear if these observations are due to subtle differences in the timing, distribution, or levels of functional AP-2α and AP-2ß protein in these tissues, or possibly different post-translational modification or functional partners for these proteins. One notable observation, though, is that no unique and irreplaceable function exists for any AP-2α/ß heterodimers in the mouse ectoderm or neural crest. This conclusion is based on the finding that loss of *Tfap2b*—a situation that would impact both AP-2ß homodimers and AP-2α/ß heterodimers—does not impact facial development in these experiments. Finally, the sensitivity of facial development to changes in the allelic dosage of the AP-2 proteins makes this gene family a potential contributor to the evolution of facial shape. Indeed, this conjecture is supported by studies comparing genetic and morphological changes in different threespine stickleback (Erickson, Baek, Hart, Cleves, & Miller, 2018) and Arctic charr (Ahi et al., 2015) populations adapted to diverse environmental conditions, as well as by comparative studies of IPS-derived cranial neural crest cells from human and chimp, which suggest that changes in AP-2 expression and/or gene targets correlates with facial shape changes (Prescott et al., 2015).

The severe EDKO phenotypes also indicated that the presence or absence of these AP-2 transcription factors in the ectoderm must have a profound influence on chromatin dynamics and gene expression. To probe this in depth, ATAC-seq, H3K4me3 ChIP-seq, and RNAseq were performed on control samples derived from the embryonic mouse face, to correlate respectively chromatin accessibility, active promoter marks, and gene expression. These datasets revealed chromatin signatures that were tissue generic as well as a subset that were specific for the E11.5 facial ectoderm with the latter enriched for P53/P63/P73, AP-2, TEAD, GRHL, and PBX binding motifs. In this respect

binding motifs for P53, AP-2, and TEAD family members have previously been found associated with ectodermal-specific gene regulatory pathways in embryonic skin (Fan et al., 2018; Wang et al., 2006; Wang et al., 2008; Yuan et al., 2020). Notably, our studies extend and refine the previous genome-wide analysis of embryonic skin conducted by Fan et al., 2018 by focusing on the E11.5 facial ectoderm, enabling the detection of additional binding motifs for GRHL and PBX TF family members that are critical craniofacial patterning genes. We complemented the analysis of control samples by performing equivalent ATAC-seq and RNAseq studies on EDKO facial ectoderm or whole facial prominences, respectively. Deletion of these two transcription factors led to a significant (5%) genome-wide loss of chromatin accessibility that was centered on AP-2 consensus motifs, particularly in potential distal enhancer elements. Despite changes in the accessibility of AP-2 binding sites, motifs for P53 and TEAD family members were still highly enriched in the EDKO mutant samples. These observations provide support for previous ATAC-seq analysis of deltaNp63 mutants which hypothesized that the AP-2 and p63 programs may function independently at the protein level to regulate chromatin accessibility in embryonic ectoderm (Fan et al., 2018). Many of the genes linked to AP-2 binding motifs were associated with annotations aligned to skin development, such as keratins, cadherins and gap junction proteins. However, further analysis of the gene list also revealed an evolutionary conserved group of AP-2 binding motifs connected with Wnt related genes, many associated with craniofacial development.

A strong link between AP-2 function, skin development, and Wnt pathway expression was also detected in the RNAseq datasets. Changes between control and EDKO mutants in the expression of various keratin genes as well *Gjb6*, *Trp63*, *Grhl3* and *Lin28a* suggest a failure or delay in appropriate skin differentiation in the latter embryos. Further, loss of AP-2α/ß caused a significant reduction in expression of many Wnt ligands within the facial ectoderm including *Wnt3*, *Wnt6*, *Wnt9b* and *Wnt10a*. Importantly, these four Wnt genes have been associated with human orofacial clefting (Reynolds et al., 2019), and alterations of *Wnt9b* also cause mouse CL/P (Juriloff et al., 2005; Juriloff, Harris, McMahon, Carroll, & Lidral, 2006). The reduced output of Wnt signaling from the ectoderm was matched by a significant reduction of *Axin2-LacZ* reporter expression in the underlying mesenchyme, and there were also multiple changes in additional Wnt components in the mesenchyme suggesting that loss of ectodermal AP-2 expression has significantly disrupted the function of this pathway throughout the

developing face. Note that, although Wnt ligand expression is reduced in the ectoderm of EDKO mutants, it is not completely lost. Therefore, the facial pathology is not as severe as that observed with the ectodermal loss of *Wls*, a gene required for Wnt ligand modification and secretion, in which the majority of the face is absent (Goodnough et al., 2014). The presence of teeth in the EDKO mutants (Woodruff, Gutierrez, Van Otterloo, Williams, & Cohn, 2021)—although abnormal in position and number—also argues against a catastrophic loss of Wnt signaling within the oral ectoderm. Further studies will be required to assess how the loss of *Tfap2a* and *Tfap2b* in the ectoderm effect other structures that require ectodermal WNT function, such as hair, whiskers and mammary buds. With respect to facial development, additional evidence for a contribution of the Wnt signaling pathway to the AP-2 mutant phenotype was obtained by overexpressing Wnt1 in the EDKO mutant background, which resulted in a significant rescue of the facial dysmorphology and clefting. A previous study also indicated that ectopic Wnt1 expression could rescue CL/P caused by loss of PBX expression (Ferretti et al., 2011), suggesting either that reduced Wnt signaling is a common pathogenic mechanism for clefting or that facial growth stimulated by excess Wnt signaling can mitigate the defects in juxtaposition and fusion of the facial prominences. Note that normal facial morphology was not fully recapitulated in the EDKO rescue experiments, possibly reflecting that the timing and level of Wnt1 expression was not adequate, or that AP-2 directs additional ectodermal programs that also contribute to face formation including IRX and IRF TF expression as well as CXCL, EDN, FGF and NOTCH signaling. Importantly, *IRF6*—a gene involved in orofacial clefting (Kondo et al., 2002; Zucchero et al., 2004)—has previously been identified as a critical AP-2 target. Studies in human have shown that a polymorphism in an upstream enhancer element either generates or disrupts binding of AP-2 proteins, with the latter variant increasing the risk for orofacial clefting (Rahimov et al., 2008). This enhancer is conserved in the mouse, and its accessibility is altered in the EDKO mutant. Further, the expression of *Irf6* is also reduced in the EDKO mutants (Table S3), correlating with the loss of AP-2 binding, and providing a further pathway that might contribute to the overall phenotype. In summary, the combination of ATAC-seq, ChIP-Seq, and expression analyses highlight critical genes that are impacted by loss of AP-2 transcription factors. These data greatly expand our understanding of the gene regulatory circuits occurring in the ectoderm that regulate facial development and underscore a critical role for AP-2α and AP-2ß in controlling

appropriate genome access as well as gene expression.

METHODS

Animal procedures: All experiments were conducted in accordance with all applicable guidelines and regulations, following the 'Guide for the Care and Use of Laboratory Animals of the National Institutes of Health'. The animal protocol utilized was approved by the Institutional Animal Care and Use Committee of the University of Colorado – Anschutz Medical Campus. Noon on the day a copulatory plug was present was denoted as embryonic day 0.5 (E0.5). For the majority of experiments, littermate embryos were used when comparing between genotypes. Yolk sacs or tail clips were used for genotyping. DNA for PCR was extracted using DirectPCR Lysis Reagent (Viagen Biotech) plus 10 µg/ml proteinase K (Roche), incubated overnight at 65°C, followed by heat inactivation at 85°C for 45 min. Samples were then used directly for PCR-based genotyping with primers (Table S4) at a final concentration of 200 nM using the Qiagen DNA polymerase kit, including the optional Q Buffer solution (Qiagen).

Mouse alleles and breeding schemes: The *Tfap2a* null (*Tfap2a*^{tm1Will} (Zhang et al., 1996)), and conditional alleles (*Tfap2a*$^{tm2Will/J}$ (Brewer et al., 2004)), the *Tfap2b* null (*Tfap2b*^{tm1Will}) and conditional alleles (*Tfap2b*^{tm2Will} (Martino et al., 2016; Van Otterloo et al., 2018)), as well as *Crect* transgenic mice (Schock et al., 2017), have been described previously. *Axin2*^{lacZ} (B6.129P2-*Axin2*^{tm1Wbm}/*J*) and *Wnt1*^{Ox} (*Gt(ROSA)26Sor*$^{tm2(Wnt1/Gfp)Amc/J}$) mice (Carroll et al., 2005; Lustig et al., 2002) were obtained from Jackson Laboratory (Bar Harbor, ME). EDKO experiments were performed using mice that were either *Crect; Tfap2a*$^{flox/flox}$*; Tfap2b*$^{flox/flox}$ or *Crect; Tfap2a*$^{null/flox}$*; Tfap2b*$^{null/flox}$ as indicated in the text. Similarly, EBKO mice were either *Crect; Tfap2a*$^{flox/+}$*; Tfap2b*$^{flox/flox}$ or *Crect; Tfap2a*$^{flox/+}$*; Tfap2b*$^{null/flox}$ and EAKO mice either *Crect; Tfap2a*$^{flox/flox}$*; Tfap2b*$^{flox/+}$ or *Crect; Tfap2a*$^{null/flox}$*; Tfap2b*$^{flox/+}$. We did not detect any gross morphological differences between the two types of EDKO, EAKO, or EBKO mice which differ in respect to the number of functional *Tfap2a* or *Tfap2b* alleles in tissues that do not express *Crect*. Note that the *Crect* transgene was always introduced into the experimental embryos via the sire to reduce global recombination sometimes seen with transmission from the female. In contrast, the Wnt1^{ox} allele was always introduced into the experimental embryos via the dam, to avoid premature activation of this allele in the sire as this genetic interaction was lethal.

Tissue preparation for ATAC-seq: For ATAC-seq analysis, E11.5 embryos were dissected into ice-cold PBS and associated yolk sacs used for rapid genotyping using the Extract-N-Amp Tissue PCR kit as recommended by the manufacturer (Sigma). During genotyping, the facial prominences were carefully removed from individual embryos using a pair of insulin syringes and placed in a 24-well plate with 1 mL of 1 mg/ml Dispase II (in PBS). The samples were incubated with rocking at 37°C for 30-40 minutes and then the facial ectoderm carefully dissected away from the mesenchyme into ice-cold PBS, as described (H. Li & Williams, 2013). Facial ectoderm was then centrifuged at 4°C, 500 g, for 3 minutes in a 1.5ml Eppendorf tube, washed 1x with ice-cold PBS, and then centrifuged again. Following resuspension in 750 µL of 0.25% trypsin-EDTA, samples were incubated at 37°C for 15 minutes with gentle agitation. Following addition of 750 µL of DMEM with 10% FBS to inhibit further digestion, cells were dissociated by pipetting up and down multiple times with wide orifice pipette tips. Cells were subsequently spun at 300 g for 5 minutes and washed with PBS containing 0.4% BSA, and this step was repeated twice. Finally, the cell pellet was resuspended with 50 µL of PBS and the density of the single cell suspension quantified on a hematocytometer.

ATAC-seq transposition, library preparation, and sequencing: Following genotype analysis of embryos used for facial ectoderm isolation, EDKO (*Crect; Tfap2a*$^{flox/flox}$*; Tfap2b*$^{flox/flox}$) and control littermate samples lacking *Crect* (*Tfap2a*$^{flox/+}$*; Tfap2b*$^{flox/+}$) were used for the ATAC-seq protocol, largely following procedures previously described (Buenrostro et al., 2013; Buenrostro et al., 2015; Corces et al., 2017). Briefly, 50,000 cells from each sample were pelleted at 500 g for 5 minutes at 4°C. The pellet was then resuspended in 50 µL of cold lysis buffer (10 mM Tris-HCl, pH 7.5; 10 mM NaCl; 3 mM $MgCl_2$; 0.1% NP-40, 0.1% Tween-20; 0.01% Digitonin) by gently pipetting ~4 times to release the nuclei which were then incubated on ice for 3 minutes. The sample was next spun at 500 g for 20 minutes at 4°C and the pelleted nuclei resuspended in Tagmentation mix (e.g. 25 µL 2x Nextera TD Buffer, 2.5 µL Nextera TD Enzyme, 0.1% Tween-20, 0.01% Digitonin, up to 50 µL with nuclease-free water) and placed at 37°C for 30 minutes in a thermocycler. Following transposition, samples were purified using the QIAGEN minElute PCR Purification Kit (Qiagen) and eluted with 11 µL of supplied Elution Buffer. Transposed DNA was

next indexed with a unique barcoded sequence and amplified prior to sequencing. Briefly, 10 µL of transposed DNA was mixed with the Nextera Ad1 PCR primer as well as a unique Nextera PCR primer (e.g. Ad2.x) and NEBNext HighFidelity 2x PCR Master Mix. Samples were then amplified using the following cycling parameters: [72°C, 5 min], [98°C, 30 sec], [98°C, 10 sec; 63°C, 30 sec; 72°C, 1 min (repeat 10-12 cycles)]. Following cycle 5, an aliquot of sample was removed for Sybr-green based quantification to determine the number of remaining cycles required to reach adequate amounts for sequencing without introducing over-amplification artifacts due to library saturation. Following indexing and amplification, samples were purified using two rounds of AmpureXP bead-based size selection. Library purity, integrity, and size were then confirmed using High Sensitivity D1000 ScreenTape and subsequently sequenced using the Illumina NovaSEQ6000 platform and 150 bp paired-end reads to a depth of ~75x10^6 reads per sample, carried out by the University of Colorado, Anschutz Medical Campus, Genomics and Microarray Core.

H3K4me3 histone ChIP: For H3K4me3 based histone ChIP-seq analysis, craniofacial ectoderm was first isolated from E10.5 and E11.5 wild-type mouse embryos, as previously described (H. Li & Williams, 2013). Once isolated and pooled, tissue/chromatin was crosslinked with 1% formaldehyde at RT for 10 minutes. Following crosslinking, reactions were quenched using 0.125 M glycine, followed by multiple PBS washes. Samples were subsequently frozen in liquid nitrogen and stored at -80°C. Once ~ 5 mg of tissue was collected per stage (e.g., E10.5, N = ~50 embryos; or E11.5, N = ~15 embryos), samples from multiple dissections, but similar stages, were pooled and combined with 300 µl of 'ChIP Nuclei Lysis buffer' (50 mM Tris-HCl, pH 8.0, 10 mM EDTA, 1% SDS), with 1mM PMSF and 1X proteinase inhibitor cocktail (PICT, 100X from Thermo Scientific, Prod # 1862209). Pooled tissue was resuspended completely and subsequently incubated at RT for 10 mins. Following incubation, chromatin was fragmented using a Bioruptor (Diagenode, Cat. No. UCD-200) with the following settings: High energy, 30 seconds on, 30 seconds off, with sonication for 45 mins. Following shearing, chromatin was assessed as ~100-500 bp in size. Next, a small portion of fragmented chromatin was saved as input, while the rest was diluted 1 in 5 in RIPA buffer (150 mM NaCl, 1% NP-40, 0.5% deoxycholate, 0.1% SDS, 50 mM Tris pH 8.0, 5 mM EDTA, plus PMSF and PICT) followed by the addition of 20 µl protein A/G agarose beads

(Pierce, Thermo Scientific, Prod # 20423) prewashed with RIPA buffer to eliminate non-specific binding. The pre-cleaned chromatin was then incubated with 2.5 µL of monoclonal H3K4Me3 primary antibody (Millipore, cat. #04-745), while rotating at 4°C, overnight. The following day, 20 ul protein A/G beads pre-saturated with 5 mg/ml BSA in PBS (Sigma, A-3311) were washed in RIPA buffer and subsequently added to the chromatin/antibody mix at 4°C, rotating, for 2 hours. Samples were then washed twice in RIPA, four times in Szak Wash (100 mM Tris HCl pH 8.5, 500 mM LiCl, 1% NP-40, 1% deoxycholate), twice more in RIPA followed by two TE washes (10 mM Tris HCl pH 8.0, 1 mM EDTA pH 8.0). Finally, the bead slurry was resuspended in 100µl TE and the remaining bound chromatin was eluted off the beads using 200 ul 1.5X 'Elution Buffer' (70 mM Tris HCl pH 8.0, 1 mM EDTA, 1.5% SDS) at 65°C for 5 mins. Once eluted, crosslinks were reversed by incubating ChIP'd samples and input samples at 65°C overnight in 200 mM NaCl. Samples were then subjected to 20 ug of Proteinase K digestion at 45 ºC for 1h and DNA subsequently extracted using a standard Phenol:Chloroform, EtOH-precipitation based approach. Purified, pelleted, DNA was then resuspended in 20µl water.

H3K4me3 histone ChIP-Seq library preparation and sequencing: Once purified fragments were obtained and quality and size confirmed, libraries were constructed using the Nugen ChIP Seq Library Construction Kit. Library purity, integrity, and size were then confirmed using High Sensitivity D1000 ScreenTape and subsequently sequenced using an Illumina MiSEQ platform and 50 bp single-end reads to a depth of ~25-30x10^6 reads per experimental sample and ~10x10^6 reads for input, carried out by the University of Colorado, Anschutz Medical Campus, Genomics and Microarray Core.

Bioinformatic processing of ATAC-seq and histone ChIP-seq data:

ATAC-seq trimming, mapping, peak calling: Following sequencing and demultiplexing, paired-end reads from each sample were first trimmed using NGmerge (with the adapter-removal flag specified) (Gaspar, 2018). Following trimming, samples were individually mapped to the Mm10 genome using Bowtie2 (Langmead, Trapnell, Pop, & Salzberg, 2009) with the following settings (--very-sensitive -k 10) and converted to bam format and sorted using Samtools (H. Li et al., 2009). To find sites of 'enrichment' (i.e. peak calling) we used Genrich (https://github.com/jsh58/Genrich) with the following flags set (-j, -y, -r, -e

chrM). First to identify control peaks, we used the two control replicate ATAC-seq alignment files—produced from Bowtie2/Samtools—as 'experimental input', with the above Genrich settings (in this approach, 'background' is based on the size of the analyzed genome, i.e., Mm10, minus mitochondrial DNA). We did a similar analysis using the two mutant replicate alignment files as 'experimental input' (rather than control)—identifying significantly enriched regions in the mutant dataset. Additionally, to compare the two datasets directly, we supplied the two control alignment files as 'experimental' while simultaneously supplying the two mutant alignment files as 'background', thus, identifying regions that were significantly enriched in controls relative to mutants. These analyses resulted in genomic coordinates of 'peaks' for each of the supplied datasets.

H3K4me3 histone ChIP-seq trimming, mapping, and overlapping: Following sequencing, samples were demultiplexed and mapped to the Mm10 genome build using NovoAlign (Novocraft). Mapped reads were then processed for duplicate removal using the Picard suite of tools (http://broadinstitute.github.io/picard). The resulting deduplicated mapped reads were subsequently indexed using Samtools (H. Li et al., 2009) and the resulting indexed Bam files were normalized using the *bamCoverage* function in deepTools (Ramirez et al., 2016). The resulting normalized bigWig files were then used with the control ATAC-seq bed file (genomic coordinates of peaks), along with the *computeMatrix* function in deepTools, to generate a matrix file. This matrix was then visualized using the *plotHeatmap* function in deepTools with a K-means cluster setting of 2, identifying ATAC-seq coordinates that had high or little to no H3K4me3 enrichment.

Multi-organ ATAC-seq dataset overlapping: First, publicly available ATAC-seq datasets were downloaded from the ENCODE consortium in bigWig file format (E11.5 heart: ENCSR820ACB; E11.5 liver: ENCSR785NEL; E11.5 hindbrain: ENCSR012YAB; E11.5 midbrain: ENCSR382RUC; E11.5 forebrain: ENCSR273UFV; E11.5 neural tube: ENCSR282YTE; E15.5 kidney: ENCSR023QZX; E15.5 intestine: ENCSR983JWA). A matrix file was then generated using all bigWig files along with the genomic coordinates obtained from the H3K4me3 clustering above (specifically the coordinates from the H3K4me3 negative cluster) using the *computeMatrix* function in deepTools. Once generated, the matrix

file was then visualized using the *plotHeatmap* function, with a K-means cluster setting of 3, in deepTools.

GREAT analysis: To determine and plot the general distribution of sub-clusters and their genomic coordinates relative to transcriptional start site of genes, the GREAT algorithm (v4) (McLean et al., 2010) was used with default settings. GREAT was also utilized for identifying enriched biological pathways and gene sets within discrete sub-clusters, with the 'Association rule settings' limited to 100 kb distal in the 'Basal plus extension' setting.

Motif enrichment analysis: For motif enrichment analysis, genomic coordinates were supplied in BED file format to the HOMER software package (Heinz et al., 2010), using the "findMotifsGenome.pl" program and default settings.

Association of gene expression and ATAC-seq peaks: First, gene expression for the craniofacial ectoderm and mesenchyme, at E11.5, was calculated using our publicly available datasets profiling the facial ectoderm and mesenchyme from E10.5 through E12.5 (Hooper et al., 2020) (available through the Facebase Consortium website, www.facebase.org, under the accession number FB00000867). Expression values for all 3 craniofacial prominences (e.g. mandibular, maxillary, frontonasal) were averaged independently for the ectoderm and mesenchyme, establishing an 'expression value' for each tissue compartment of the entire face at E11.5. Next, an 'ectoderm enrichment' value was calculated for each gene by taking the quotient of the ectoderm value divided by the mesenchyme value. Concurrently, ATAC-seq peaks from various sub-clusters were associated with a corresponding gene(s) using the GREAT algorithm and these associations were downloaded using the '*Gene -> genomic regions association table*' function in GREAT. A 'peak-associated profile' was then ascribed for each gene (i.e., the type and number of sub-cluster peaks associated with each gene), allowing the binning of genes based on this profile. Bins of genes, and their associated 'ectoderm enrichment' value were then plotted in R using the empirical cumulative distribution function (stat_ecdf) in ggplot2 and significance calculated using a Kolmogorov-Smirnov test (ks.test).

Conservation analysis: To determine the level of conversation for AP-2 dependent genomic elements (Figure 3E) the phastCons60way (scores for multiple alignments of 59 vertebrate genomes to the mouse genome) dataset was downloaded from the University of California, Santa Cruz (UCSC) genome browser in bigWig format (http://hgdownload.cse.ucsc.edu/goldenpath/mm10/phastCons60way/). A matrix file was then generated using the bigWig file along with the 'AP-2 dependent' genomic coordinates using the *computeMatrix* function in deepTools. Once generated, the matrix file was then visualized using the *plotHeatmap* function, with a K-means cluster setting of 2, in deepTools.

RNA-sequencing:

For RNA-sequencing E10.5 facial prominences encompassing ectoderm and mesenchyme of the mandibular, maxillary, and nasal prominences were micro-dissected in ice cold PBS using insulin syringes and stored in RNA-later at -20°C. Once sufficient EDKO (*Crect; Tfap2a*$^{flox/null}$*; Tfap2b*$^{flox/null}$) and control littermate samples lacking *Crect* (e.g. *Tfap2a*$^{flox/+}$*; Tfap2b*$^{flox/+}$) were identified for 3 biological replicates of each, tissue was removed from RNA-later and RNA harvested as previously described using the microRNA Purification Kit (Norgen Biotek) and following manufacturer's protocol (Van Otterloo et al., 2018). Following elution, mRNA was further purified using the Qiagen RNAeasy Kit according to the manufacturer's protocol. The quality of extracted mRNA was assessed using DNA Analysis ScreenTape (Agilent Technologies) prior to library production. Following validation of extracted mRNA, cDNA libraries were generated using the Illumina TruSeq Stranded mRNA Sample Prep Kit. All libraries passed quality control guidelines and were then sequenced using the Illumina HiSeq2500 platform and single-end reads (1×150) to a depth of ~15-25x10^6 reads per sample. To identify differentially expressed genes between control and mutant groups, we next utilized a standard bioinformatic pipeline for read filtering, mapping, gene expression quantification, and differential expression between groups (see below). Library construction and sequencing was carried out by the University of Colorado, Anschutz Medical Campus, Genomics and Microarray Core.

Bioinformatic processing of RNA-seq data: Raw sequencing reads were demultiplexed and fastq files subsequently processed, as previously described (Van Otterloo et al., 2018). Briefly, reads were trimmed

using the Java software package Trim Galore! (Babraham Bioinformatics, Babraham Institute, Cambridge, UK) and subsequently mapped to the Mm10 genome using the HISAT2 software package (Pertea, Kim, Pertea, Leek, & Salzberg, 2016) (both with default settings). Following mapping, RNA expression levels were generated using StringTie (Pertea et al., 2016) and differential expression computed between genotypes using CuffDiff2 (Trapnell et al., 2012), with a significance cut-off value of Q<0.05 (FDR-corrected P-value). As a secondary approach, particularly for plotting differential gene expression differences for specific transcripts (e.g., Figure 7J), quantification of transcript abundance was calculated using kallisto (Bray, Pimentel, Melsted, & Pachter, 2016) and then compared and visualized using sleuth (Pimentel, Bray, Puente, Melsted, & Pachter, 2017).

Skeletal staining: Concurrent staining of bone and cartilage in E18.5 embryos occurred as previously described (Van Otterloo et al., 2016). Briefly, following euthanasia and removal of skin and viscera, embryos were first dehydrated in 95% EtOH and then for ~2 days in 100% Acetone. Embryos were then incubated in a mixture of alcian blue, alizarin red, acetic acid (5%) and 70% EtOH, at 37°C, for ~2-3 days. Samples were then placed in 2% KOH (~1-2 days) and then 1% KOH (~1-2 days) to allow for clearing of remaining soft tissue. Final skeletal preparations were stored at 4°C in 20% glycerol. Staining of only cartilage in E15.5 embryos occurred as previously reported (Van Otterloo et al., 2016). Briefly, following fixation in Bouin's at 4°C overnight, embryos were washed with repeated changes of 70% EtOH and 0.1% NH_4OH until all traces of Bouin's coloration was removed. Tissue was permeabilized by two 1 hr washes in 5% acetic acid, followed by overnight incubation in a solution of methylene blue (0.05%) and acetic acid (5%). Next, embryos were washed twice with 5% acetic acid (~1hr each wash) and then twice with 100% MeOH (~1hr each wash). Finally, embryos were cleared with a solution consisting of one-part benzyl alcohol and two parts benzyl benzoate (BABB).

***In situ* hybridization**: Embryos were fixed overnight in 4% PFA at 4°C and then dehydrated through a graded series of MeOH:PBST washes and stored in 100% MeOH at -20°C. Prior to hybridization they were rehydrated from MeOH into PBST as previously described (Simmons, Bolanis, Wang, & Conway, 2014; Van Otterloo et al., 2016). Note, for some experiments, embryonic heads were bisected in a mid-

964 sagittal plane, with either half being used with a unique anti-sense RNA probes. At a minimum, each *in situ* probe examined was run on 3 control and 3 EDKO mutant embryos. Antisense RNA probes were
966 generated using a unique fragment that was cloned into a TOPO vector (Life Technologies, Grand Island, NY), using cDNA synthesized from mouse embryonic mRNA as a template. cDNA was generated
968 using the SuperScript® III First-Strand Synthesis System (Life Technologies, Grand Island, NY), as per manufacturer's instructions. The *Wnt3* probe is equivalent to nucleotides 674-1727 of NM_009521.2;
970 *Wnt9b* to nucleotides 1158- 2195 of NM_011719; *Kremen2* probe is equivalent to nucleotides 206-832 of NM_028416. Sequence verified plasmids were linearized and antisense probes synthesized using an
972 appropriate DNA-dependent RNA polymerase (T7/T3/SP6) and DIG RNA labeling mix (Roche, Basel, Switzerland).

974

Cell proliferation analysis: To analyze cell proliferation in sectioned mouse embryos, E11.5 embryos
976 were harvested and fixed overnight in 4% PFA at 4°C. The following day, embryos were moved through a series of PBS and sucrose washes, followed by a mixture of sucrose and OCT. Embryos were then
978 transferred to a plastic mold containing 100% OCT. After orientating the tissue samples in the plastic molds, the OCT ‘block’ was frozen on dry ice and stored at -80°C. OCT blocks, containing control and
980 mutant embryos, were then sectioned at 12 µM on a cryostat. Sectioned materials were stored at -80°C. For immunolabeling, slides which contained the frontonasal, maxillary, or mandibular prominence were
982 brought to room temperature, washed 4 x 15 minutes in PBST, blocked for 1 hr in PBST plus 3% milk. Sections were then incubated overnight in primary antibody (anti-p-Histone H3, sc-8656-R, Santa Cruz
984 Biotechnology, rabbit polyclonal) diluted 1:250 in PBST at 4°C in a humidified chamber. Following primary antibody incubation, samples were washed twice for 10 min in PBST at room temperature,
986 followed by a 30 min wash in PBST/3% milk. Samples were then incubated for 1 h with a secondary antibody (goat anti-rabbit IgG, Alexa Flour 488 conjugate, ThermoFisher Scientific/Invitrogen, R37116)
988 and DRAQ5 (Abcam, ab108410) nuclear stain, diluted 1:250 and 1:5000, respectively, in PBST. Processed samples were imaged on a Leica TCS SP5 II confocal microscope and individual images
990 taken for visualization. After acquiring an image of each prominence, the area of interest was outlined in Image-J and immuno-positive cells within that area were counted by an independent observer—who was

blinded to the sample genotype—using the *threshold* and *particle counter* function. The number of positive cells/area of the 'area of interest' (e.g., the prominence) was then calculated for sections originating from 3 control and 3 EDKO embryos. An unpaired student T-test was used to assess statistical significance between groups.

ß-galactosidase staining: Whole-mount ß-galactosidase staining was conducted as previously described (Seberg et al., 2017). Briefly, embryos were fixed for ~30 minutes to 1 hour at RT in PBS containing 0.25% glutaraldehyde, washed 3 x 30 minutes in a 'lacZ rinse buffer' followed by enzymatic detection using a chromogenic substrate (1 mg/ml X-gal) diluted in a 'lacZ staining solution'. Staining in embryos was developed at 37°C until an optimal intensity was observed, embryos were then rinsed briefly in PBS, and then post-fixed in 4% PFA overnight.

Real-time PCR: Real-time reverse transcriptase PCR was carried out, essentially as previously described (Van Otterloo et al., 2018). Briefly, embryos were harvested at the indicated stage and facial prominences dissected off for RNA isolation. Tissue was stored in RNAlater at −20°C until genotyping was completed on samples. Following positive identification of genotypes, tissue was equilibrated at 4°C for 1 day, RNAlater removed, and RNA extracted from tissue samples using the Rneasy Plus Mini Kit (Qiagen) along with the optional genomic DNA eliminator columns. Following RNA isolation and quantification, cDNA was generated using a set amount of RNA and the SuperScript III First-Strand Synthesis Kit (Invitrogen/ThermoFisher Scientific). Once cDNA was generated, quantitative real-time PCR analysis was conducted using a Bio-Rad CFX Connect instrument, Sybr Select Master Mix (Applied Biosystems, ThermoFisher Scientific) and 20 µl reactions (all reactions performed in triplicate). All primers were designed to target exons flanking (when available) large intronic sequences. Relative mRNA expression levels were quantified using the $^{\Delta\Delta}$Ct method (Dussault & Pouliot, 2006) and an internal relative control (β-actin).

Scanning Electron Microscopy: Specimens were processed for electron microscopy according to standardized procedures. Briefly, the samples were fixed in glutaraldehyde, rinsed in sodium cacodylate buffer, and secondarily fixed in osmium tetroxide before dehydrating in a graduated ethanol series. Following dehydration, the samples were mounted on a SEM stub and sputter coated for 30 seconds

using a gold/palladium target in a Lecia (Buffalo Grove, IL) EM ACE 200 Vacuum Coater. Scanning electron micrographs were acquired using a JEOL (Peabody, MA) JSM-6010LA electron microscope operated in high-vacuum mode at 20kV.

ACKNOWLEDGEMENTS:

The authors would like to acknowledge Irene Choi, for her care and maintenance of the animal colonies utilized in this study, and Eric Wartchow for assistance with electron microscopy. We are grateful to our colleagues at the University of Colorado, Anschutz Medical Campus, Department of Craniofacial Biology as well as and the University of Iowa, Department of Anatomy and Cell Biology, for their valuable critiques and feedback. We thank the Genomics Shared Resource at the University of Colorado Cancer Center for assistance with next-generation sequencing.

And finally, our funding sources, including the National Institute of Dental and Craniofacial Research.

NIDCR K99/R00 DE026823 to EVO, and NIH 2R01 DE12728 to TW.

COMPETING INTERESTS:

All authors declare no competing interests.

SUPPLEMENTAL FIGURE LEGENDS

Supplemental Figure 1. Summary of motif enrichment found within H3K4me3+ ATAC-seq elements (i.e., Figure 2D, top).

Supplemental Figure 2. Summary of motif enrichment found within H3K4me3- ATAC-seq elements (i.e., Figure 2D, bottom).

Supplemental Figure 3. Summary of GREAT analysis of H3K4me3+ ATAC-seq elements.

Supplemental Figure 4. Summary of GREAT analysis of H3K4me3- ATAC-seq elements.

Supplemental Figure 5. Summary of motif enrichment found within C1 ATAC-seq elements (i.e., Figure 2E, top).

Supplemental Figure 6. Summary of GREAT analysis of C1 ATAC-seq elements (i.e., Figure 2E, top).

Supplemental Figure 7. Summary of motif enrichment found within C3 ATAC-seq elements (i.e., Figure 2E, bottom).

Supplemental Figure 8. Summary of GREAT analysis of C3 ATAC-seq elements (i.e., Figure 2E, bottom).

Supplemental Figure 9. Summary of motif enrichment found within C2 ATAC-seq elements (i.e., Figure 2E, middle).

Supplemental Figure 10. Summary of GREAT analysis of C2 ATAC-seq elements (i.e., Figure 2E, middle).

Supplemental Figure 11. A cumulative distribution plot graphing E11.5 craniofacial gene expression enrichment (ectoderm/mesenchyme, X-axis) relative to the total number of C2 and C3 ATAC-seq elements associated with that gene.

Supplemental Figure 12. Summary of motif enrichment found within ATAC-seq elements remaining in EDKO mutant surface ectoderm.

Supplemental Figure 13. Summary of motif enrichment found within ATAC-seq elements that are AP-2 dependent (i.e., present in control, but gone in EDKO) in the craniofacial surface ectoderm.

Supplemental Figure 14. Summary of GREAT analysis using ATAC-seq elements that are AP-2 dependent (i.e., present in control, but gone in EDKO) in the craniofacial surface ectoderm.

Supplemental Figure 15. Summary of GREAT analysis using ATAC-seq elements that are AP-2 dependent (i.e., present in control, but gone in EDKO) in the craniofacial surface ectoderm and are 'ultra-conserved' (i.e., Figure 3E, Top).

Supplemental Figure 16. Summary of GREAT analysis using ATAC-seq elements that are AP-2 dependent (i.e., present in control, but gone in EDKO) in the craniofacial surface ectoderm and are 'non-ultra-conserved' (i.e., Figure 3E, Bottom).

Supplemental Figure 17. Summary of motif enrichment found within ATAC-seq elements that are gained upon loss of AP-2 in the craniofacial surface ectoderm (i.e., element not found in control, but present in EDKO).

Supplemental Figure 18. IGV browser screenshot of ATAC-seq tracks at the *Sostdc1* locus. Black tracks are control samples (e.g., ctrl 1, ctrl 2), while green tracks are EDKO samples (e.g., mut 1, mut2). Green boxes below EDKO samples represent ATAC-seq regions that are significantly reduced in EDKO's vs controls.

Supplemental Figure 19. IGV browser screenshot of ATAC-seq tracks near *the Axin2* locus. AP-2 dependent peaks are located ~160kb upstream of the Axin2 promoter (located at ~108,920) within introns of the adjacent *Cep112* gene. Black tracks are control samples (e.g., ctrl 1, ctrl 2), while green tracks are EDKO samples (e.g., mut 1, mut2). Green boxes below EDKO samples represent ATAC-seq regions that are significantly reduced in EDKO's vs controls.

Supplemental Figure 20. Bar-charts summarizing real-time RT-PCR analysis of cDNA generated from RNA collected from E11.5 craniofacial mesenchyme (mes) or surface ectoderm (ect) of a control or EDKO (mut) sample. Relative expression (normalized to ß-actin) is shown for both Wnt3 (expressed only in the ectoderm) and Axin2 (expressed in both ectoderm and mesenchyme).

Supplemental Figure 21. (**A-B**) Boxplots summarizing quantification of the number of anti-phospho histone H3+ cells per area, of either control (grey) or EDKO (red) E11.5 embryos, either collectively within a section of the face (i.e., all prominences) (A) or by each prominence individually (B). The mean is indicated by the unfilled circle, 75th and 25th percentiles by the limits of the box, and the largest or smallest value within 1.5 times the interquartile range by the lines. Outliers are indicated by the isolated points. A standard two-tailed t-test was conducted to calculate significance.

Supplemental Figure 22. Scatterplot as described for Figure 7E. Briefly, the plot highlights gene expression changes (X-axis) in the facial prominences of EDKO (α/ßCRECT) versus control (CTRL) samples. Genes are further stratified based on their given enrichment in the surface ectoderm versus mesenchyme (Y-axis) in a control embryo. All WNT-pathway components (as defined by DAVID pathway analysis) have been labeled sky-blue.

Supplemental Figure 23. Real-time RT-PCR (A, D, G) or in situ hybridization (B, C, E, F) of various Wnt pathway components in E10.5 control (ctrl), EAKO (αCRECT), or EDKO (α/ßCRECT) embryos. cDNA for real-time PCR was generated from RNA collected from either the medial and lateral nasal prominences or the combined MxP and MnP portions of the face as diagrammed, from the given genotype. In situ hybridization images show a representative E10.5 embryo in a lateral view of the head.

Supplemental Table 1. Summary of gene expression values in the craniofacial surface ectoderm versus the facial mesenchyme of wild-type E11.5 mouse embryos and the association of these genes with the ATAC-seq elements identified in Figure 2E, the promoter distal peaks (used for cumulative distribution plotting).

Supplemental Table 2. Summary of ATAC-seq element gene association for the AP-2 dependent peaks. For each gene, the total number of elements (both promoter proximal and distal) and genomic location of each element, relative to the transcriptional start site, are indicated.

Supplemental Table 3. Gene expression summary for E10.5 RNA-seq analysis of control and EDKO facial prominence samples. Note, each tab of the spreadsheet contains a subset of the larger dataset that was used for further analysis.

Supplemental Table 4. Summary of primers used for the current study.

References

Ahi, E. P., Steinhauser, S. S., Palsson, A., Franzdottir, S. R., Snorrason, S. S., Maier, V. H., & Jonsson, Z. O. (2015). Differential expression of the aryl hydrocarbon receptor pathway associates with craniofacial polymorphism in sympatric Arctic charr. *Evodevo, 6*, 27. doi:10.1186/s13227-015-0022-6

Andersson, R., & Sandelin, A. (2020). Determinants of enhancer and promoter activities of regulatory elements. *Nat Rev Genet, 21*(2), 71-87. doi:10.1038/s41576-019-0173-8

Badis, G., Berger, M. F., Philippakis, A. A., Talukder, S., Gehrke, A. R., Jaeger, S. A., . . . Bulyk, M. L. (2009). Diversity and complexity in DNA recognition by transcription factors. *Science, 324*(5935), 1720-1723. doi:10.1126/science.1162327

Bebee, T. W., Park, J. W., Sheridan, K. I., Warzecha, C. C., Cieply, B. W., Rohacek, A. M., . . . Carstens, R. P. (2015). The splicing regulators Esrp1 and Esrp2 direct an epithelial splicing program essential for mammalian development. *Elife, 4*. doi:10.7554/eLife.08954

Bosher, J. M., Totty, N. F., Hsuan, J. J., Williams, T., & Hurst, H. C. (1996). A family of AP-2 proteins regulates c-erbB-2 expression in mammary carcinoma. *Oncogene, 13*(8), 1701-1707. Retrieved from https://www.ncbi.nlm.nih.gov/pubmed/8895516

Bray, N. L., Pimentel, H., Melsted, P., & Pachter, L. (2016). Near-optimal probabilistic RNA-seq quantification. *Nat Biotechnol, 34*(5), 525-527. doi:10.1038/nbt.3519

Brewer, S., Feng, W., Huang, J., Sullivan, S., & Williams, T. (2004). Wnt1-Cre-mediated deletion of AP-2alpha causes multiple neural crest-related defects. *Dev Biol, 267*(1), 135-152. doi:10.1016/j.ydbio.2003.10.039

Buenrostro, J. D., Giresi, P. G., Zaba, L. C., Chang, H. Y., & Greenleaf, W. J. (2013). Transposition of native chromatin for fast and sensitive epigenomic profiling of open chromatin, DNA-binding proteins and nucleosome position. *Nat Methods, 10*(12), 1213-1218. doi:10.1038/nmeth.2688

Buenrostro, J. D., Wu, B., Chang, H. Y., & Greenleaf, W. J. (2015). ATAC-seq: A Method for Assaying Chromatin Accessibility Genome-Wide. *Curr Protoc Mol Biol, 109*, 21 29 21-21 29 29. doi:10.1002/0471142727.mb2129s109

Carroll, T. J., Park, J. S., Hayashi, S., Majumdar, A., & McMahon, A. P. (2005). Wnt9b plays a central role in the regulation of mesenchymal to epithelial transitions underlying organogenesis of the mammalian urogenital system. *Dev Cell, 9*(2), 283-292. doi:10.1016/j.devcel.2005.05.016

Celli, J., Duijf, P., Hamel, B. C., Bamshad, M., Kramer, B., Smits, A. P., . . . van Bokhoven, H. (1999). Heterozygous germline mutations in the p53 homolog p63 are the cause of EEC syndrome. *Cell, 99*(2), 143-153. doi:10.1016/s0092-8674(00)81646-3

Chai, Y., & Maxson, R. E., Jr. (2006). Recent advances in craniofacial morphogenesis. *Dev Dyn, 235*(9), 2353-2375. doi:10.1002/dvdy.20833

Chen, E. Y., Tan, C. M., Kou, Y., Duan, Q., Wang, Z., Meirelles, G. V., . . . Ma'ayan, A. (2013). Enrichr: interactive and collaborative HTML5 gene list enrichment analysis tool. *BMC Bioinformatics, 14*, 128. doi:10.1186/1471-2105-14-128

Chiquet, B. T., Blanton, S. H., Burt, A., Ma, D., Stal, S., Mulliken, J. B., & Hecht, J. T. (2008). Variation in WNT genes is associated with non-syndromic cleft lip with or without cleft palate. *Hum Mol Genet, 17*(14), 2212-2218. doi:10.1093/hmg/ddn121

Consortium, E. P. (2012). An integrated encyclopedia of DNA elements in the human genome. *Nature, 489*(7414), 57-74. doi:10.1038/nature11247

Corces, M. R., Trevino, A. E., Hamilton, E. G., Greenside, P. G., Sinnott-Armstrong, N. A., Vesuna, S., . . . Chang, H. Y. (2017). An improved ATAC-seq protocol reduces background and enables interrogation of frozen tissues. *Nat Methods, 14*(10), 959-962. doi:10.1038/nmeth.4396

Davies, A. F., Stephens, R. J., Olavesen, M. G., Heather, L., Dixon, M. J., Magee, A., . . . Ragoussis, J. (1995). Evidence of a locus for orofacial clefting on human chromosome 6p24 and STS content map of the region. *Hum Mol Genet, 4*(1), 121-128. doi:10.1093/hmg/4.1.121

Davies, S. J., Wise, C., Venkatesh, B., Mirza, G., Jefferson, A., Volpi, E. V., & Ragoussis, J. (2004). Mapping of three translocation breakpoints associated with orofacial clefting within 6p24 and identification of new transcripts within the region. *Cytogenet Genome Res, 105*(1), 47-53. doi:10.1159/000078008

Davis, C. A., Hitz, B. C., Sloan, C. A., Chan, E. T., Davidson, J. M., Gabdank, I., . . . Cherry, J. M. (2018). The Encyclopedia of DNA elements (ENCODE): data portal update. *Nucleic Acids Res, 46*(D1), D794-D801. doi:10.1093/nar/gkx1081

Dixon, J. R., Selvaraj, S., Yue, F., Kim, A., Li, Y., Shen, Y., . . . Ren, B. (2012). Topological domains in mammalian genomes identified by analysis of chromatin interactions. *Nature, 485*(7398), 376-380. doi:10.1038/nature11082

Dixon, M. J., Marazita, M. L., Beaty, T. H., & Murray, J. C. (2011). Cleft lip and palate: understanding genetic and environmental influences. *Nat Rev Genet, 12*(3), 167-178. doi:10.1038/nrg2933

Dussault, A. A., & Pouliot, M. (2006). Rapid and simple comparison of messenger RNA levels using real-time PCR. *Biol Proced Online, 8*, 1-10. doi:10.1251/bpo114

Eckert, D., Buhl, S., Weber, S., Jager, R., & Schorle, H. (2005). The AP-2 family of transcription factors. *Genome Biol, 6*(13), 246. doi:10.1186/gb-2005-6-13-246

Erickson, P. A., Baek, J., Hart, J. C., Cleves, P. A., & Miller, C. T. (2018). Genetic Dissection of a Supergene Implicates Tfap2a in Craniofacial Evolution of Threespine Sticklebacks. *Genetics, 209*(2), 591-605. doi:10.1534/genetics.118.300760

Fan, X., Wang, D., Burgmaier, J. E., Teng, Y., Romano, R. A., Sinha, S., & Yi, R. (2018). Single Cell and Open Chromatin Analysis Reveals Molecular Origin of Epidermal Cells of the Skin. *Dev Cell, 47*(1), 21-37 e25. doi:10.1016/j.devcel.2018.08.010

Feng, W., Simoes-de-Souza, F., Finger, T. E., Restrepo, D., & Williams, T. (2009). Disorganized olfactory bulb lamination in mice deficient for transcription factor AP-2epsilon. *Mol Cell Neurosci, 42*(3), 161-171. doi:10.1016/j.mcn.2009.06.010

Ferretti, E., Li, B., Zewdu, R., Wells, V., Hebert, J. M., Karner, C., . . . Selleri, L. (2011). A conserved Pbx-Wnt-p63-Irf6 regulatory module controls face morphogenesis by promoting epithelial apoptosis. *Dev Cell, 21*(4), 627-641. doi:10.1016/j.devcel.2011.08.005

Gaspar, J. M. (2018). NGmerge: merging paired-end reads via novel empirically-derived models of sequencing errors. *BMC Bioinformatics, 19*(1), 536. doi:10.1186/s12859-018-2579-2

Goodnough, L. H., Dinuoscio, G. J., Ferguson, J. W., Williams, T., Lang, R. A., & Atit, R. P. (2014). Distinct requirements for cranial ectoderm and mesenchyme-derived wnts in specification and differentiation of osteoblast and dermal progenitors. *PLoS Genet, 10*(2), e1004152. doi:10.1371/journal.pgen.1004152

Guttormsen, J., Koster, M. I., Stevens, J. R., Roop, D. R., Williams, T., & Winger, Q. A. (2008). Disruption of epidermal specific gene expression and delayed skin development in AP-2 gamma mutant mice. *Dev Biol, 317*(1), 187-195. doi:10.1016/j.ydbio.2008.02.017

Heinz, S., Benner, C., Spann, N., Bertolino, E., Lin, Y. C., Laslo, P., . . . Glass, C. K. (2010). Simple combinations of lineage-determining transcription factors prime cis-regulatory elements required for macrophage and B cell identities. *Mol Cell, 38*(4), 576-589. doi:10.1016/j.molcel.2010.05.004

Hesse, K., Vaupel, K., Kurt, S., Buettner, R., Kirfel, J., & Moser, M. (2011). AP-2delta is a crucial transcriptional regulator of the posterior midbrain. *PLoS One, 6*(8), e23483. doi:10.1371/journal.pone.0023483

Hicks, E. A., Zaveri, M., Deschamps, P. A., Noseworthy, M. D., Ball, A., Williams, T., & West-Mays, J. A. (2018). Conditional Deletion of AP-2alpha and AP-2beta in the Developing Murine Retina Leads to Altered Amacrine Cell Mosaics and Disrupted Visual Function. *Invest Ophthalmol Vis Sci, 59*(6), 2229-2239. doi:10.1167/iovs.17-23283

Hoffman, T. L., Javier, A. L., Campeau, S. A., Knight, R. D., & Schilling, T. F. (2007). Tfap2 transcription factors in zebrafish neural crest development and ectodermal evolution. *J Exp Zool B Mol Dev Evol, 308*(5), 679-691. doi:10.1002/jez.b.21189

Hong, S. J., Lardaro, T., Oh, M. S., Huh, Y., Ding, Y., Kang, U. J., . . . Kim, K. S. (2008). Regulation of the noradrenaline neurotransmitter phenotype by the transcription factor AP-2beta. *J Biol Chem, 283*(24), 16860-16867. doi:10.1074/jbc.M709106200

Hooper, J. E., Jones, K. L., Smith, F. J., Williams, T., & Li, H. (2020). An Alternative Splicing Program for Mouse Craniofacial Development. *Front Physiol, 11*, 1099. doi:10.3389/fphys.2020.01099

Hu, D., & Marcucio, R. S. (2009). Unique organization of the frontonasal ectodermal zone in birds and mammals. *Dev Biol, 325*(1), 200-210. doi:10.1016/j.ydbio.2008.10.026

Hu, D., Marcucio, R. S., & Helms, J. A. (2003). A zone of frontonasal ectoderm regulates patterning and growth in the face. *Development, 130*(9), 1749-1758. doi:10.1242/dev.00397

Imai, K. S., Hikawa, H., Kobayashi, K., & Satou, Y. (2017). Tfap2 and Sox1/2/3 cooperatively specify

ectodermal fates in ascidian embryos. *Development, 144*(1), 33-37. doi:10.1242/dev.142109

Jiang, R., Lan, Y., Chapman, H. D., Shawber, C., Norton, C. R., Serreze, D. V., . . . Gridley, T. (1998). Defects in limb, craniofacial, and thymic development in Jagged2 mutant mice. *Genes Dev, 12*(7), 1046-1057. doi:10.1101/gad.12.7.1046

Jin, Y. R., Han, X. H., Taketo, M. M., & Yoon, J. K. (2012). Wnt9b-dependent FGF signaling is crucial for outgrowth of the nasal and maxillary processes during upper jaw and lip development. *Development, 139*(10), 1821-1830. doi:10.1242/dev.075796

Juriloff, D. M., Harris, M. J., Dewell, S. L., Brown, C. J., Mager, D. L., Gagnier, L., & Mah, D. G. (2005). Investigations of the genomic region that contains the clf1 mutation, a causal gene in multifactorial cleft lip and palate in mice. *Birth Defects Res A Clin Mol Teratol, 73*(2), 103-113. doi:10.1002/bdra.20106

Juriloff, D. M., Harris, M. J., McMahon, A. P., Carroll, T. J., & Lidral, A. C. (2006). Wnt9b is the mutated gene involved in multifactorial nonsyndromic cleft lip with or without cleft palate in A/WySn mice, as confirmed by a genetic complementation test. *Birth Defects Res A Clin Mol Teratol, 76*(8), 574-579. doi:10.1002/bdra.20302

Knight, R. D., Javidan, Y., Zhang, T., Nelson, S., & Schilling, T. F. (2005). AP2-dependent signals from the ectoderm regulate craniofacial development in the zebrafish embryo. *Development, 132*(13), 3127-3138. doi:10.1242/dev.01879

Kondo, S., Schutte, B. C., Richardson, R. J., Bjork, B. C., Knight, A. S., Watanabe, Y., . . . Murray, J. C. (2002). Mutations in IRF6 cause Van der Woude and popliteal pterygium syndromes. *Nat Genet, 32*(2), 285-289. doi:10.1038/ng985

Kuleshov, M. V., Jones, M. R., Rouillard, A. D., Fernandez, N. F., Duan, Q., Wang, Z., . . . Ma'ayan, A. (2016). Enrichr: a comprehensive gene set enrichment analysis web server 2016 update. *Nucleic Acids Res, 44*(W1), W90-97. doi:10.1093/nar/gkw377

Langmead, B., Trapnell, C., Pop, M., & Salzberg, S. L. (2009). Ultrafast and memory-efficient alignment of short DNA sequences to the human genome. *Genome Biol, 10*(3), R25. doi:10.1186/gb-2009-10-3-r25

Le Douarin, N. M., Creuzet, S., Couly, G., & Dupin, E. (2004). Neural crest cell plasticity and its limits. *Development, 131*(19), 4637-4650. doi:10.1242/dev.01350

Leach, S. M., Feng, W., & Williams, T. (2017). Gene expression profile data for mouse facial development. *Data Brief, 13*, 242-247. doi:10.1016/j.dib.2017.05.003

Lee, S., Kong, Y., & Weatherbee, S. D. (2013). Forward genetics identifies Kdf1/1810019J16Rik as an essential regulator of the proliferation-differentiation decision in epidermal progenitor cells. *Dev Biol, 383*(2), 201-213. doi:10.1016/j.ydbio.2013.09.022

Lee, S., Sears, M. J., Zhang, Z., Li, H., Salhab, I., Krebs, P., . . . Carstens, R. P. (2020). Cleft lip and cleft palate in Esrp1 knockout mice is associated with alterations in epithelial-mesenchymal crosstalk. *Development, 147*(21). doi:10.1242/dev.187369

Leslie, E. J., Liu, H., Carlson, J. C., Shaffer, J. R., Feingold, E., Wehby, G., . . . Marazita, M. L. (2016). A Genome-wide Association Study of Nonsyndromic Cleft Palate Identifies an Etiologic Missense Variant in GRHL3. *Am J Hum Genet, 98*(4), 744-754. doi:10.1016/j.ajhg.2016.02.014

Li, H., Handsaker, B., Wysoker, A., Fennell, T., Ruan, J., Homer, N., . . . Genome Project Data Processing, S. (2009). The Sequence Alignment/Map format and SAMtools. *Bioinformatics, 25*(16), 2078-2079. doi:10.1093/bioinformatics/btp352

Li, H., & Williams, T. (2013). Separation of mouse embryonic facial ectoderm and mesenchyme. *J Vis Exp*(74). doi:10.3791/50248

Li, L., Wang, Y., Torkelson, J. L., Shankar, G., Pattison, J. M., Zhen, H. H., . . . Oro, A. E. (2019). TFAP2C- and p63-Dependent Networks Sequentially Rearrange Chromatin Landscapes to Drive Human Epidermal Lineage Commitment. *Cell Stem Cell, 24*(2), 271-284 e278. doi:10.1016/j.stem.2018.12.012

Li, W., & Cornell, R. A. (2007). Redundant activities of Tfap2a and Tfap2c are required for neural crest induction and development of other non-neural ectoderm derivatives in zebrafish embryos. *Dev Biol, 304*(1), 338-354. doi:10.1016/j.ydbio.2006.12.042

Lustig, B., Jerchow, B., Sachs, M., Weiler, S., Pietsch, T., Karsten, U., . . . Behrens, J. (2002). Negative feedback loop of Wnt signaling through upregulation of conductin/axin2 in colorectal and liver tumors. *Mol Cell Biol, 22*(4), 1184-1193. doi:10.1128/mcb.22.4.1184-1193.2002

Martino, V. B., Sabljic, T., Deschamps, P., Green, R. M., Akula, M., Peacock, E., . . . West-Mays, J. A.

(2016). Conditional deletion of AP-2beta in mouse cranial neural crest results in anterior segment dysgenesis and early-onset glaucoma. *Dis Model Mech, 9*(8), 849-861. doi:10.1242/dmm.025262

McLean, C. Y., Bristor, D., Hiller, M., Clarke, S. L., Schaar, B. T., Lowe, C. B., . . . Bejerano, G. (2010). GREAT improves functional interpretation of cis-regulatory regions. *Nat Biotechnol, 28*(5), 495-501. doi:10.1038/nbt.1630

Menezes, R., Letra, A., Kim, A. H., Kuchler, E. C., Day, A., Tannure, P. N., . . . Vieira, A. R. (2010). Studies with Wnt genes and nonsyndromic cleft lip and palate. *Birth Defects Res A Clin Mol Teratol, 88*(11), 995-1000. doi:10.1002/bdra.20720

Meulemans, D., & Bronner-Fraser, M. (2002). Amphioxus and lamprey AP-2 genes: implications for neural crest evolution and migration patterns. *Development, 129*(21), 4953-4962. Retrieved from https://www.ncbi.nlm.nih.gov/pubmed/12397104

Meulemans, D., & Bronner-Fraser, M. (2004). Gene-regulatory interactions in neural crest evolution and development. *Dev Cell, 7*(3), 291-299. doi:10.1016/j.devcel.2004.08.007

Milunsky, J. M., Maher, T. A., Zhao, G., Roberts, A. E., Stalker, H. J., Zori, R. T., . . . Lin, A. E. (2008). TFAP2A mutations result in branchio-oculo-facial syndrome. *Am J Hum Genet, 82*(5), 1171-1177. doi:10.1016/j.ajhg.2008.03.005

Minoux, M., Holwerda, S., Vitobello, A., Kitazawa, T., Kohler, H., Stadler, M. B., & Rijli, F. M. (2017). Gene bivalency at Polycomb domains regulates cranial neural crest positional identity. *Science, 355*(6332). doi:10.1126/science.aal2913

Minoux, M., & Rijli, F. M. (2010). Molecular mechanisms of cranial neural crest cell migration and patterning in craniofacial development. *Development, 137*(16), 2605-2621. doi:10.1242/dev.040048

Mitchell, J. M., Sucharov, J., Pulvino, A. T., Brooks, E. P., Gillen, A. E., & Nichols, J. T. (2021). The alx3 gene shapes the zebrafish neurocranium by regulating frontonasal neural crest cell differentiation timing. *Development*. doi:10.1242/dev.197483

Moser, M., Pscherer, A., Roth, C., Becker, J., Mucher, G., Zerres, K., . . . Fassler, R. (1997). Enhanced apoptotic cell death of renal epithelial cells in mice lacking transcription factor AP-2beta. *Genes Dev, 11*(15), 1938-1948. doi:10.1101/gad.11.15.1938

Nyberg, D. A., Hegge, F. N., Kramer, D., Mahony, B. S., & Kropp, R. J. (1993). Premaxillary protrusion: a sonographic clue to bilateral cleft lip and palate. *J Ultrasound Med, 12*(6), 331-335. Retrieved from https://www.ncbi.nlm.nih.gov/pubmed/8515530

Ong, C. T., & Corces, V. G. (2014). CTCF: an architectural protein bridging genome topology and function. *Nat Rev Genet, 15*(4), 234-246. doi:10.1038/nrg3663

Pertea, M., Kim, D., Pertea, G. M., Leek, J. T., & Salzberg, S. L. (2016). Transcript-level expression analysis of RNA-seq experiments with HISAT, StringTie and Ballgown. *Nat Protoc, 11*(9), 1650-1667. doi:10.1038/nprot.2016.095

Peyrard-Janvid, M., Leslie, E. J., Kousa, Y. A., Smith, T. L., Dunnwald, M., Magnusson, M., . . . Schutte, B. C. (2014). Dominant mutations in GRHL3 cause Van der Woude Syndrome and disrupt oral periderm development. *Am J Hum Genet, 94*(1), 23-32. doi:10.1016/j.ajhg.2013.11.009

Pimentel, H., Bray, N. L., Puente, S., Melsted, P., & Pachter, L. (2017). Differential analysis of RNA-seq incorporating quantification uncertainty. *Nat Methods, 14*(7), 687-690. doi:10.1038/nmeth.4324

Pontoriero, G. F., Deschamps, P., Ashery-Padan, R., Wong, R., Yang, Y., Zavadil, J., . . . West-Mays, J. A. (2008). Cell autonomous roles for AP-2alpha in lens vesicle separation and maintenance of the lens epithelial cell phenotype. *Dev Dyn, 237*(3), 602-617. doi:10.1002/dvdy.21445

Prescott, S. L., Srinivasan, R., Marchetto, M. C., Grishina, I., Narvaiza, I., Selleri, L., . . . Wysocka, J. (2015). Enhancer divergence and cis-regulatory evolution in the human and chimp neural crest. *Cell, 163*(1), 68-83. doi:10.1016/j.cell.2015.08.036

Rahimov, F., Marazita, M. L., Visel, A., Cooper, M. E., Hitchler, M. J., Rubini, M., . . . Murray, J. C. (2008). Disruption of an AP-2alpha binding site in an IRF6 enhancer is associated with cleft lip. *Nat Genet, 40*(11), 1341-1347. doi:10.1038/ng.242

Ramirez, F., Ryan, D. P., Gruning, B., Bhardwaj, V., Kilpert, F., Richter, A. S., . . . Manke, T. (2016). deepTools2: a next generation web server for deep-sequencing data analysis. *Nucleic Acids Res, 44*(W1), W160-165. doi:10.1093/nar/gkw257

Reynolds, K., Kumari, P., Sepulveda Rincon, L., Gu, R., Ji, Y., Kumar, S., & Zhou, C. J. (2019). Wnt signaling in orofacial clefts: crosstalk, pathogenesis and models. *Dis Model Mech, 12*(2). doi:10.1242/dmm.037051

Richardson, R. J., Dixon, J., Malhotra, S., Hardman, M. J., Knowles, L., Boot-Handford, R. P., . . . Dixon, M. J. (2006). Irf6 is a key determinant of the keratinocyte proliferation-differentiation switch. *Nat Genet, 38*(11), 1329-1334. doi:10.1038/ng1894

Rothstein, M., & Simoes-Costa, M. (2020). Heterodimerization of TFAP2 pioneer factors drives epigenomic remodeling during neural crest specification. *Genome Res, 30*(1), 35-48. doi:10.1101/gr.249680.119

Satoda, M., Zhao, F., Diaz, G. A., Burn, J., Goodship, J., Davidson, H. R., . . . Gelb, B. D. (2000). Mutations in TFAP2B cause Char syndrome, a familial form of patent ductus arteriosus. *Nat Genet, 25*(1), 42-46. doi:10.1038/75578

Schmidt, M., Huber, L., Majdazari, A., Schutz, G., Williams, T., & Rohrer, H. (2011). The transcription factors AP-2beta and AP-2alpha are required for survival of sympathetic progenitors and differentiated sympathetic neurons. *Dev Biol, 355*(1), 89-100. doi:10.1016/j.ydbio.2011.04.011

Schock, E. N., Struve, J. N., Chang, C. F., Williams, T. J., Snedeker, J., Attia, A. C., . . . Brugmann, S. A. (2017). A tissue-specific role for intraflagellar transport genes during craniofacial development. *PLoS One, 12*(3), e0174206. doi:10.1371/journal.pone.0174206

Schorle, H., Meier, P., Buchert, M., Jaenisch, R., & Mitchell, P. J. (1996). Transcription factor AP-2 essential for cranial closure and craniofacial development. *Nature, 381*(6579), 235-238. doi:10.1038/381235a0

Seberg, H. E., Van Otterloo, E., Loftus, S. K., Liu, H., Bonde, G., Sompallae, R., . . . Cornell, R. A. (2017). TFAP2 paralogs regulate melanocyte differentiation in parallel with MITF. *PLoS Genet, 13*(3), e1006636. doi:10.1371/journal.pgen.1006636

Simmons, O., Bolanis, E. M., Wang, J., & Conway, S. J. (2014). In situ hybridization (both radioactive and nonradioactive) and spatiotemporal gene expression analysis. *Methods Mol Biol, 1194*, 225-244. doi:10.1007/978-1-4939-1215-5_12

Smith, A. N., Miller, L. A., Song, N., Taketo, M. M., & Lang, R. A. (2005). The duality of beta-catenin function: a requirement in lens morphogenesis and signaling suppression of lens fate in periocular ectoderm. *Dev Biol, 285*(2), 477-489. doi:10.1016/j.ydbio.2005.07.019

Ting, S. B., Caddy, J., Hislop, N., Wilanowski, T., Auden, A., Zhao, L. L., . . . Jane, S. M. (2005). A homolog of Drosophila grainy head is essential for epidermal integrity in mice. *Science, 308*(5720), 411-413. doi:10.1126/science.1107511

Trapnell, C., Roberts, A., Goff, L., Pertea, G., Kim, D., Kelley, D. R., . . . Pachter, L. (2012). Differential gene and transcript expression analysis of RNA-seq experiments with TopHat and Cufflinks. *Nat Protoc, 7*(3), 562-578. doi:10.1038/nprot.2012.016

Van Otterloo, E., Feng, W., Jones, K. L., Hynes, N. E., Clouthier, D. E., Niswander, L., & Williams, T. (2016). MEMO1 drives cranial endochondral ossification and palatogenesis. *Dev Biol, 415*(2), 278-295. doi:10.1016/j.ydbio.2015.12.024

Van Otterloo, E., Li, H., Jones, K. L., & Williams, T. (2018). AP-2alpha and AP-2beta cooperatively orchestrate homeobox gene expression during branchial arch patterning. *Development, 145*(2). doi:10.1242/dev.157438

Van Otterloo, E., Li, W., Bonde, G., Day, K. M., Hsu, M. Y., & Cornell, R. A. (2010). Differentiation of zebrafish melanophores depends on transcription factors AP2 alpha and AP2 epsilon. *PLoS Genet, 6*(9), e1001122. doi:10.1371/journal.pgen.1001122

Van Otterloo, E., Li, W., Garnett, A., Cattell, M., Medeiros, D. M., & Cornell, R. A. (2012). Novel Tfap2-mediated control of soxE expression facilitated the evolutionary emergence of the neural crest. *Development, 139*(4), 720-730. doi:10.1242/dev.071308

Wang, X., Bolotin, D., Chu, D. H., Polak, L., Williams, T., & Fuchs, E. (2006). AP-2alpha: a regulator of EGF receptor signaling and proliferation in skin epidermis. *J Cell Biol, 172*(3), 409-421. doi:10.1083/jcb.200510002

Wang, X., Pasolli, H. A., Williams, T., & Fuchs, E. (2008). AP-2 factors act in concert with Notch to orchestrate terminal differentiation in skin epidermis. *J Cell Biol, 183*(1), 37-48. doi:10.1083/jcb.200804030

Watanabe, A., Akita, S., Tin, N. T., Natsume, N., Nakano, Y., Niikawa, N., . . . Yoshiura, K. (2006). A mutation in RYK is a genetic factor for nonsyndromic cleft lip and palate. *Cleft Palate Craniofac J, 43*(3), 310-316. doi:10.1597/04-145.1

Williams, T., & Tjian, R. (1991). Analysis of the DNA-binding and activation properties of the human transcription factor AP-2. *Genes Dev, 5*(4), 670-682. doi:10.1101/gad.5.4.670

Woodruff, E. D., Gutierrez, G. C., Van Otterloo, E., Williams, T., & Cohn, M. J. (2021). Anomalous incisor morphology indicates tissue-specific roles for Tfap2a and Tfap2b in tooth development. *Dev Biol, 472*, 67-74. doi:10.1016/j.ydbio.2020.12.017

Yuan, Y., Park, J., Feng, A., Awasthi, P., Wang, Z., Chen, Q., & Iglesias-Bartolome, R. (2020). YAP1/TAZ-TEAD transcriptional networks maintain skin homeostasis by regulating cell proliferation and limiting KLF4 activity. *Nat Commun, 11*(1), 1472. doi:10.1038/s41467-020-15301-0

Zainolabidin, N., Kamath, S. P., Thanawalla, A. R., & Chen, A. I. (2017). Distinct Activities of Tfap2A and Tfap2B in the Specification of GABAergic Interneurons in the Developing Cerebellum. *Front Mol Neurosci, 10*, 281. doi:10.3389/fnmol.2017.00281

Zhang, J., Hagopian-Donaldson, S., Serbedzija, G., Elsemore, J., Plehn-Dujowich, D., McMahon, A. P., . . . Williams, T. (1996). Neural tube, skeletal and body wall defects in mice lacking transcription factor AP-2. *Nature, 381*(6579), 238-241. doi:10.1038/381238a0

Zhao, F., Bosserhoff, A. K., Buettner, R., & Moser, M. (2011). A heart-hand syndrome gene: Tfap2b plays a critical role in the development and remodeling of mouse ductus arteriosus and limb patterning. *PLoS One, 6*(7), e22908. doi:10.1371/journal.pone.0022908

Zhao, F., Satoda, M., Licht, J. D., Hayashizaki, Y., & Gelb, B. D. (2001). Cloning and characterization of a novel mouse AP-2 transcription factor, AP-2delta, with unique DNA binding and transactivation properties. *J Biol Chem, 276*(44), 40755-40760. doi:10.1074/jbc.M106284200

Zucchero, T. M., Cooper, M. E., Maher, B. S., Daack-Hirsch, S., Nepomuceno, B., Ribeiro, L., . . . Murray, J. C. (2004). Interferon regulatory factor 6 (IRF6) gene variants and the risk of isolated cleft lip or palate. *N Engl J Med, 351*(8), 769-780. doi:10.1056/NEJMoa032909